Wang S, Li J, Zhang B, Spyrakos E, Tyler AN, Shen Q, Zhang F, Kuster T, Lehmann MK, Wu Y & Peng D (2018) Trophic state assessment of global inland waters using a MODIS-derived Forel-Ule index. *Remote Sensing of Environment*, 217, pp. 444-460.

DOI: 10.1016/j.rse.2018.08.026

Trophic state assessment of global inland waters using a MODIS-derived Forel-Ule index

Shenglei Wang[a,b,c], Junsheng Li[a,b], Bing Zhang[a,b,*], Evangelos Spyrakos[c], Andrew N. Tyler[c], Qian Shen[a], Fangfang Zhang[a], Tiit Kuster[d], Moritz K. Lehmann[e], Yanhong Wu[a], Dailiang Peng[a]

[a]*Key Laboratory of Digital Earth, Instituteof Remote Sensing and Digital Earth, Chinese Academy of Sciences, Beijing100094, China*

[b]*University of Chinese Academy of Sciences, Beijing 100049, China*

[c]*Biological and Environmental Sciences, School of Natural Sciences, University of Stirling, Stirling, United Kingdom*

[d]*Estonian Marine Institute, University of Tartu, Mäealuse 14, Tallinn, 12618, Estonia*

[e]*Environmental Research Institute, University of Waikato, Hamilton, New Zealand*

[*]*Corresponding author, e-mail address:* zb@radi.ac.cn

Abstract

Eutrophication of inland waters is considered a serious global environmental problem. Satellite remote sensing (RS) has been established as an important source of information to determine the trophic state of inland waters through the retrieval of optically active water quality parameters such as chlorophyll-a (Chl-a). However, the use of RS techniques for assessment of the trophic state of inland waters on a global scale is hindered by the performance of retrieval algorithms over highly dynamic and complex optical properties that characterize many of these systems. In this study, we developed a new RS approach to assess the trophic state of global inland water bodies based on Moderate Resolution Imaging Spectroradiometer (MODIS) imagery and the Forel-Ule index (FUI). First, the FUI was calculated from MODIS data by dividing natural water colour into 21 indices from dark blue to yellowish-brown. Then the relationship between FUI and the trophic state index (TSI) was established based on in-situ measurements and MODIS products. The water-leaving reflectance at 645 nm band was employed to distinguish coloured dissolved organic matter (CDOM)-dominated systems in the FUI-based trophic state assessment. Based on the analysis, the FUI-based trophic state assessment method was developed and applied to assess the trophic states of 2058 large inland water bodies (surface area > 25 km^2) distributed around the world using MODIS data from the austral and boreal summers of 2012. Our results showed that FUI can be retrieved from MODIS with a considerable accuracy (92.5%, R^2=0.92) by comparing with concurrent in situ measurements over a wide range of lakes, and the overall accuracy of the FUI-based trophic state assessment method is 80.0% (R^2 = 0.75) validated by an independent dataset. Of the global large water bodies considered, oligotrophic large lakes were found to be concentrated in plateau regions in central Asia and southern South America, while eutrophic large lakes were concentrated in central Africa, eastern Asia, and mid-northern and southeast North America.

Keywords: trophic state, global inland waters, Forel-Ule index, MODIS

1. Introduction

Eutrophication represents a serious water quality challenge around the world (Jones and Lee, 1982; Le et al., 2010; Smith, 2003; Vollenweider, 1981). This process is often associated with the rapid production of phytoplankton and other microorganisms, which have important impacts on aquatic ecology and the normal functioning of water bodies (Vollenweider and Kerekes, 1982). The trophic state of inland waters is typically categorized into three levels: oligotrophic, mesotrophic, and eutrophic. Since the 1960s, attempts have been made to quantitatively evaluate the trophic state of inland waters using both single-variable and multi-variable methods (Beeton and Edmondson, 1972; Bigham Stephens et al., 2015; Burns and Bryers, 2000; Forsberg and Ryding, 1980; Rodhe, 1969). Carlson (1977) introduced a numerical *Trophic State Index* (TSI) for inland waters based on algae biomass, which can be calculated using Secchi depth (SD), chlorophyll-a (Chl-a), or total phosphorus (TP). Many studies have used Chl-a, a pigment common to almost all photosynthetic organisms, as a proxy for algal biomass and therefore also as an indicator for the trophic state of aquatic systems (Carlson, 1991; Joniak et al., 2009; Sheela et al., 2011a). The Trophic Level Index (TLI), another commonly used numerical method, is calculated from the weighted sum of either three variables (Chl-a, TP, total nitrogen (TN)) or five variables with the addition of SD and chemical oxygen demand (COD) (Burns and Bryers, 2000; Burns et al., 1999; Jin and Tu, 1990; Verburg et al., 2010).

Collecting systematic observations on the ecological status of inland waters in aquatic systems in inland waters remains a logistical and financial challenge which with conventional in-situ approaches scales proportionately with increasing geographical coverage (Härmä et al., 2001; Hu et al., 2010; McClain, 2009). However, satellite based remote sensing (RS) offers a potentially significant source of information for large-scale monitoring of water state variables (including water trophic state).

Eutrophication and increased productivity typically result in changes in the optical properties of water; therefore, RS approaches have been employed for water trophic state assessment (Baban, 1996; Papoutsa et al., 2014), in particular through the retrieval of Chl-a concentrations (Chen, 2003; Duan et al., 2007; Matthews and Odermatt, 2015; Pulliainen et al., 2001; Thiemann and Kaufmann, 2000; Wang et al., 2008). In addition, SD, which is one of the most commonly measured trophic state indicators, has also been used to assess water trophic states (Binding et al., 2015; Knight and Voth, 2012; Lillesand et al., 1983; Olmanson et al., 2008; Papoutsa et al., 2014; Sheela et al., 2011b). Other studies based on RS have used multiple variables to assess water trophic states (Cheng and Lei, 2001; Sass et al., 2007; Xiang et al., 2015). However, most of the RS-based retrieval methods make assumptions about the biogeo-optical properties of the target aquatic system and have spatial-temporal limitations or high demands on the spectral resolution of RS data, due to the complex optical properties of inland waters (Shen et al., 2014; Spyrakos et al., 2018; Ylöstalo et al., 2014). An additional challenge is the calculation of water-leaving reflectance ($R_{rs}(\lambda)$) data globally by removing various and complex atmospheric effects (Chen et al., 2013a; Wang et al., 2016), although several atmospheric correction models have been developed to overcome the atmospheric correction problems for different types of inland waters (Hu et al., 2000; Shanmugam and Ahn, 2007; Wang and Shi, 2007; Wang et al., 2011; Zhang et al., 2014). Given these challenges, the development of a globally valid Earth observation approach for water trophic state assessment has been hindered (Palmer et al., 2015).

Here, we promote a water colour index, Forel-Ule index (FUI), as the water quality parameter to assess trophic state of inland waters. We chose the FUI, which divides natural waters into 21 colour classes from dark blue to yellowish brown based on the traditional Forel-Ule scale due to its wide covering of water optical characteristics and intimate relations with water quality (Wernand and Van der Woerd, 2010; Van der Woerd et al., 2016). Indeed, water colour expressed through a single colour index is generally not sufficient to retrieve variables such as Chl-a or suspended sediments unambiguously (Bukata, 1983; Bukata 1995). However, studies have demonstrated that water colour is closely associated with the absorption and scattering effects of water constituents (including Chl-a and suspended sediments), and therefore can be used to reflect the comprehensive water quality (Garaba et al., 2014; Wang et al., 2015; Wernand et al., 2013a). Since the FUI can be objectively retrieved using RS observations at the global scale (Li et al., 2016; Wernand et al., 2013b), it could provide a feasible solution to monitoring global inland water bodies.

The main aim of this study was to develop an FUI-based trophic state assessment approach for global inland waters using the Moderate-resolution Imaging Spectroradiometer (MODIS) data, and to provide a global-scale view of the water quality of large lakes and reservoirs worldwide.

2. Datasets

2.1 MODIS surface reflectance product

The MODIS level-3 surface reflectance product (MOD09A1) provides data of mapped surface spectral reflectance at 500 m spatial resolution from 7 bands across the visible and near infrared and short-wave infrared wavelengths (i.e. 469 , 555, 645, 859, 1240, 1640, and 2130 nm) (Vermote and Vermeulen, 1999). MOD09A1 is an 8-day composite MODIS Terra product, which is spatially divided by uniform MODIS tiles on the global scale, which makes it easy to calculate global time-series statistics. It has been used for long-term and large-area water quality monitoring research as this dataset is well georeferenced, synthesized, and cloud marked (Hou et al., 2017; Klein et al., 2017; Li et al., 2016; Wu et al., 2013).

In order to retrieve the FUI of global inland waters, we used more than 6400 MOD09A1 images taken during the summer months of 2012 acquired from the Goddard Space Flight Center (GSFC) of the National Aeronautics and Space Administration (NASA) (http://ladsweb.nascom.nasa.gov/index.html). We chose the year 2012 because of the availability of validation data from published studies and online databases about the trophic state of inland waters. Summer months (i.e. from June to September in the Northern Hemisphere, and from December to March in the Southern Hemisphere) were used to retrieve the FUI, because the biomass of Chl-a-containing planktonic algae generally peaks in this season (Singh and Singh, 2015) and therefore has the greatest effect on water colour.

2.2 In-situ dataset

Details of the field measured Chl-a and in-situ $R_{rs}(\lambda)$ are given in in Table 1. The in-situ dataset contains 469 samplings from 10 lakes in Asia, North America, and Europe. The selection represents different types of inland waters, ranging from a few oligotrophic and mesotrophic lakes to more eutrophic lakes, from lakes with high total suspended matter (TSM, i.e. Taihu Lake) to lakes with high coloured dissolved organic matter (CDOM, i.e. Lake Peipsi and Lake Winnipeg).

Table1 Lake Names, locations, number of samplings (N), mean Chl-a concentrations (Chl-a, μg/L) and data sources of the 10 lakes and reservoirs with field measurements

Lake	Latitude	Longitude	Chl-a	N	Data Source
Lake Maggiore	46.01 N	8.67 E	2.41	3	In-situ (Giardino et al., 2013)
Lake Winnipeg	51.9 N	97.3 W	5.33	58	In-situ (Binding et al., 2013)
Lake Erie	41.9 N	82.1 W	9.34	24	In-situ (Binding et al., 2013)
Lake Peipsi	58.47 N	27.34 E	17.95	26	In-situ (Kutser et al. 2013)
Lake Erhai	25.86 N	100.15 E	19.11	21	In-situ
Yuqiao Reservoir	40.04 N	117.55 E	20.73	13	In-situ
Guanting Reservoir	40.35 N	115.73 E	26.8	31	In-situ
Taihu Lake	31.20 N	120.18 E	42.6	239	In-situ
Chaohu Lake	31.55 N	117.57 E	64.47	29	In-situ
Dianchi Lake	24.82 N	102.71 E	85.2	25	In-situ

Equation (1), suggested by Carlson (1977), was applied to the Chl-a dataset:

$$\mathrm{TSI(Chl\text{-}a)} = 10\left(6 - \frac{2.04 - 0.68 \ln Chl\text{-}a}{ln2}\right) \tag{1}$$

where Chl-a denotes the concentration of Chl-a in μg/L. The TSI method classifies the water trophic state as oligotrophic (TSI < 30), mesotrophic (30 ≤ TSI < 50), or eutrophic (TSI ≥ 50). The in-situ measured $R_{rs}(\lambda)$ was used to simulate MODIS bands by using MODIS spectral response functions (SRF), and then the FUI for these samplings was calculated to determine the relationship between TSI and FUI.

Concurrent MOD09 images were acquired to build the data pairs of $R_{rs}(\lambda)$. The FUI was calculated from the data pairs and compared to evaluate the accuracy of MODIS FUI. The data pairs were coincident within a ±3 hour window and the nearest MODIS image pixel was used to pair with the in-situ data. After removing concurrent MODIS data with cloud cover, noise cover, and near shoreline pixels, there were 135 pairs of $R_{rs}(\lambda)$ data from 7 of the 10 lakes. There were 73 pairs for Taihu Lake with 13 concurrent images in July and October 2006, and January and April 2007 (Wang et al., 2016); 10 pairs for Qinghai Lake with 1 concurrent image in August 2014 (Li et al., 2016); 10 pairs for Lake Erhai with 1 concurrent image in July 2012; 17 pairs for Lake Erie (Binding et al., 2013) with 3 concurrent images in August 2012; 20 pairs for Lake Winnipeg (Binding et al., 2013) with 8 concurrent images in July and August 2012; 4 pairs for Lake Peipsi (Kutser et al., 2013) with 1 concurrent image in June 2012; and 1 pair for Lake Maggiore (Giardino et al., 2013) with 1 concurrent image in July 2012.

2.3 Hydrolight simulated dataset

A Hydrolight simulated Chl-a and $R_{rs}(\lambda)$ dataset published by (IOCCG, 2006) was also used to improve the representativeness of oligotrophic to mesotrophic waters in our dataset, and to illustrate the theoretical relationship between FUI and TSI in these relatively clear waters. This dataset was simulated using the widely accepted Hydrolight code (Mobley, 1995), with input inherent optical properties (IOPs) generated from a wide range of field measurements with various bio-optical models not limited to Case I water (IOCCG, 2006). The concentration of Chl-a in the simulated dataset ranges from 0.03 to 30.0 μg/L with an average value of 6.08 μg/L.

2.4 Independent validation dataset

The FUI-based water trophic state assessment results for the summer of 2012 were validated through comparison with published studies and online databases, including China Environmental State Bulletin from Ministry of Environmental Protection of the People's Republic of China (MEPPRC, 2012), and the National Lake Assessment from the US Environmental Protection Agency (USEPA, 2016). To guarantee objectiveness and fairness in the validation process, comparison data were only selected where they represented the whole water body, and where the acquisition time was as close as possible to the year of 2012. In total, 100 inland water bodies distributed around the globe were used for validation (Figure 1).

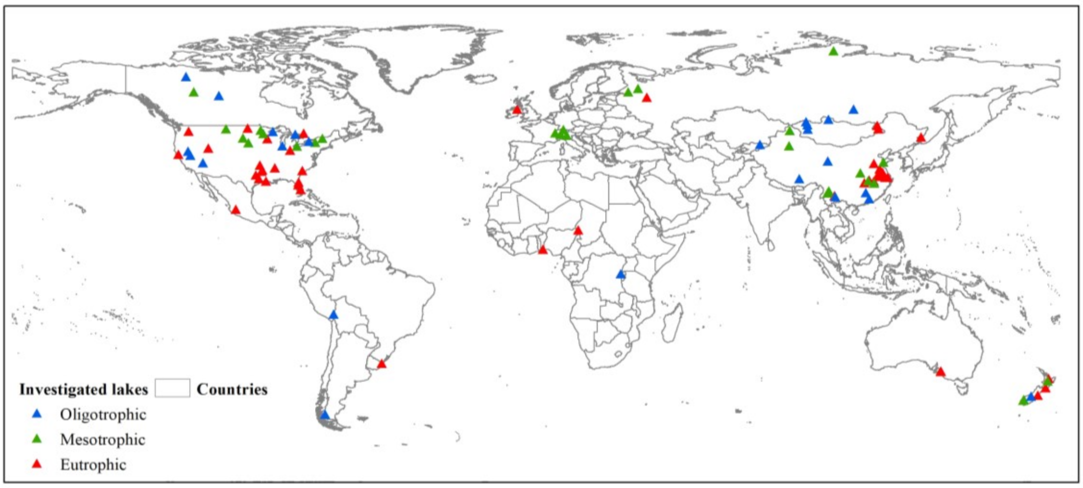

Figure 1 Spatial distribution and trophic states of 100 water bodies used for validation of the Moderate Resolution Imaging Spectroradiometer (MODIS)-derived Forel-Ule index (FUI) method. Trophic state data were obtained through literature review. Blue triangles denote oligotrophic water bodies, green triangles denote mesotrophic water bodies, and red triangles denote eutrophic water bodies.

3. Methods

3.1 Water-leaving reflectance correction

The MODIS surface reflectance products (MOD09) have been corrected for the effects of atmospheric gases, aerosols, thin cirrus clouds and adjacency from MODIS L1B data (Vermote and Vermeulen, 1999). It was found that the MOD09 reflectance was overall greater than the in situ reflectance over inland waters due to the residual noises, including the residual aerosol effect, skylight reflection, and possible sun glint (Wang, 2016). It is considered that MOD09 often fails to correct for aerosol effect because its aerosol input (the MODIS aerosol product, MOD04) usually uses a small fill value for the aerosol optical thickness for most inland waters (Wang et al., 2016; Vermote and Vermeulen, 1999). In this study, a band subtraction method based on near-infrared (NIR) to short wave infrared (SWIR) bands was used to reduce the noises in MOD09 data and to convert it to water-leaving reflectance ($R_{rs}(\lambda)$) (Wang, 2016). The correction equation is:

$$R_{\mathrm{rs}}(\lambda) = \frac{R(\lambda) - \min(R_{\mathrm{NIR}} : R_{\mathrm{SWIR}})}{\pi} \quad (2)$$

where $R(\lambda)$ is the original reflectance of the MOD09 band, and $\min(R_{NIR} : R_{SWIR})$ is the minimum positive value of the NIR and SWIR bands. The $\min(R_{NIR} : R_{SWIR})$ was subtracted from each pixel for each band to account for the residual errors (Wang and Shi, 2007; Wang, 2016). This method neglects the aerosol types, but it can also avoid the uncertainties in the NIR and SWIR bands being amplified by aerosol exponential models. The formula is divided by π to convert the surface reflectance to water-leaving reflectance by neglecting the bidirectional effects. Despite imperfections and limitations, this method has been shown to achieve accuracies around 30%, and it can be easily implemented in operational data processing systems for deriving $R_{rs}(\lambda)$ with relative stable performances over inland waters under various conditions (Wang et al., 2016).

3.2 Water body identification

The water bodies studied were large lakes and reservoirs (i.e., > 25 km^2 and covering > 100 pixels in a MOD09A1 image). Water body extraction was taken directly from satellite data rather than using a static geographic database due to the dynamic nature of margins of some water bodies. The detection of water pixels in the MOD09A1 product was carried out using a series of processing steps on the MODIS satellite data outlined in Figure 2.

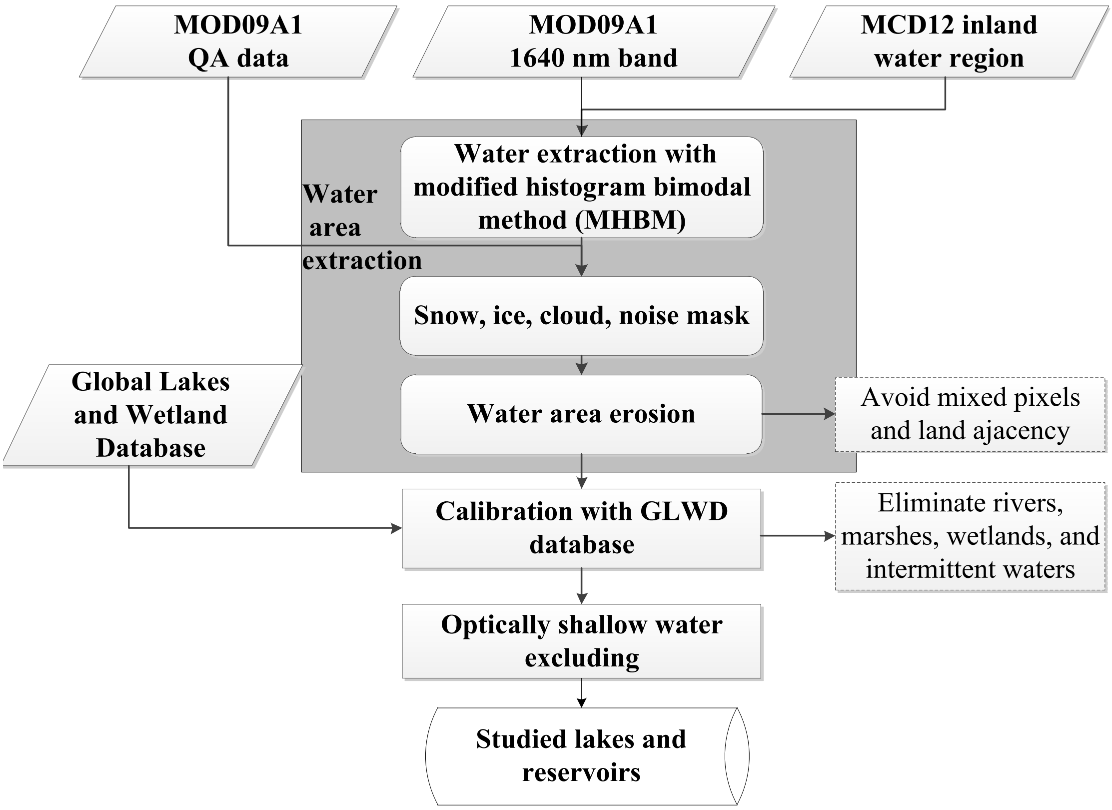

Figure 2 Flowchart of water body extraction and calibration from MOD09A1 products. MOD09A1 QA data is the Quality Assurance dataset that included in MOD09A1 dataset. MHBM is the modified histogram bimodal method suggested by Zhang et al. (2018).

3.2.1 Water body extraction and identification

The modified histogram bimodal method (MHBM) suggested by Zhang et al. (2018) was used to automatically segment water areas from land in the MOD09A1 image by using the 6th band (1640 nm) with a dynamic threshold for each water body. The 1640 nm band was selected because it was strongly absorbed by water and strongly reflected by terrestrial regions (Mishra and Prasad, 2015). There are six steps in the segmentation process as follows:

(1) For each water body, the initial water area provided by the MODIS Land Cover Type product (MCD12Q1 Type-1) (Friedl et al., 2010), which is gridded identically to MOD09A1, was extended around the coastline reaching a number of 250% pixels of the water area (including the initial water area).

(2) For each water body, a reflectance histogram of the 1640 nm band of the dilated region was calculated, and the valley value of the histogram falling in the threshold range was automatically determined as the threshold for the specific water body. The range of thresholds from a range of representative water types was 0.005 to 0.11;

(3) Water bodies were segmented from MOD09A1 images using the determined thresholds;

(4) MOD09A1 Quality Assurance (QA) data (Vermote et al., 2015) were used to eliminate cloud, ice, and snow cover, and low quality pixels from the water areas;

(5) Extracted water areas were eroded with a 500 m buffer to avoid the effects of mixed land-water pixels and severe land adjacency near the shoreline and to ensure the quality of water pixels (Hou et al., 2017);

(6) Water bodies with areas of water connected with more than 100 pixels (i.e., > 25 km^2) were selected for this study.

The 500 m buffer was determined according to the comparison of MODIS $R_{rs}(\lambda)$ in the transects selected from the land–water boundaries; it showed that generally, one pixel (500 m) near the shoreline at the visible bands was subject to detectable adjacency contamination, which is consistent with the findings of Hou et al. (2017). Notably, the land adjacency effect for MODIS may theoretically have an impact at much larger distances offshore (Bulgarelli and Zibordi, 2018), but considering that the uncertainty in MODIS $R_{rs}(\lambda)$ is already approximately 30%, the adjacency effect at distances greater than 500 m may not be obvious.

Figure 3 shows the examples of water segmentation from MOD09A1 data. It demonstrates that the water pixels have characteristically low reflectance values which aids in detection against different land cover types, including small islands (Figure 3 (b) and (c)), clouds (Figure 3 (f) and (g)), snow and ice (Figure 3 (e)), aquatic plants (Figure 3 (g)) and low quality pixels (Figure 3 (g)). The $R_{rs}(1640)$ values of the intersect lines (marked in Figure 3) under different conditions are shown in Figure 4.

The extracted water areas were intersected with the Global Lakes and Wetland Database (GLWD) (Lehner and Döll, 2004), which represents a compilation of numerous existing maps and datasets and has been validated comprehensively for lakes > 1 km^2. GLWD Level 3 (GLWD-3) comprises lakes, reservoirs, rivers and different wetland types in the form of a global raster map at 30-second resolution. Since the aim of this study is to assess the trophic state of lakes and reservoirs at the global scale, water bodies with centroid points located in the lake or reservoir type in the GLWD-3 database were chosen, and those located in rivers, ephemeral waters, coastal wetland

and other types of wetland were removed.

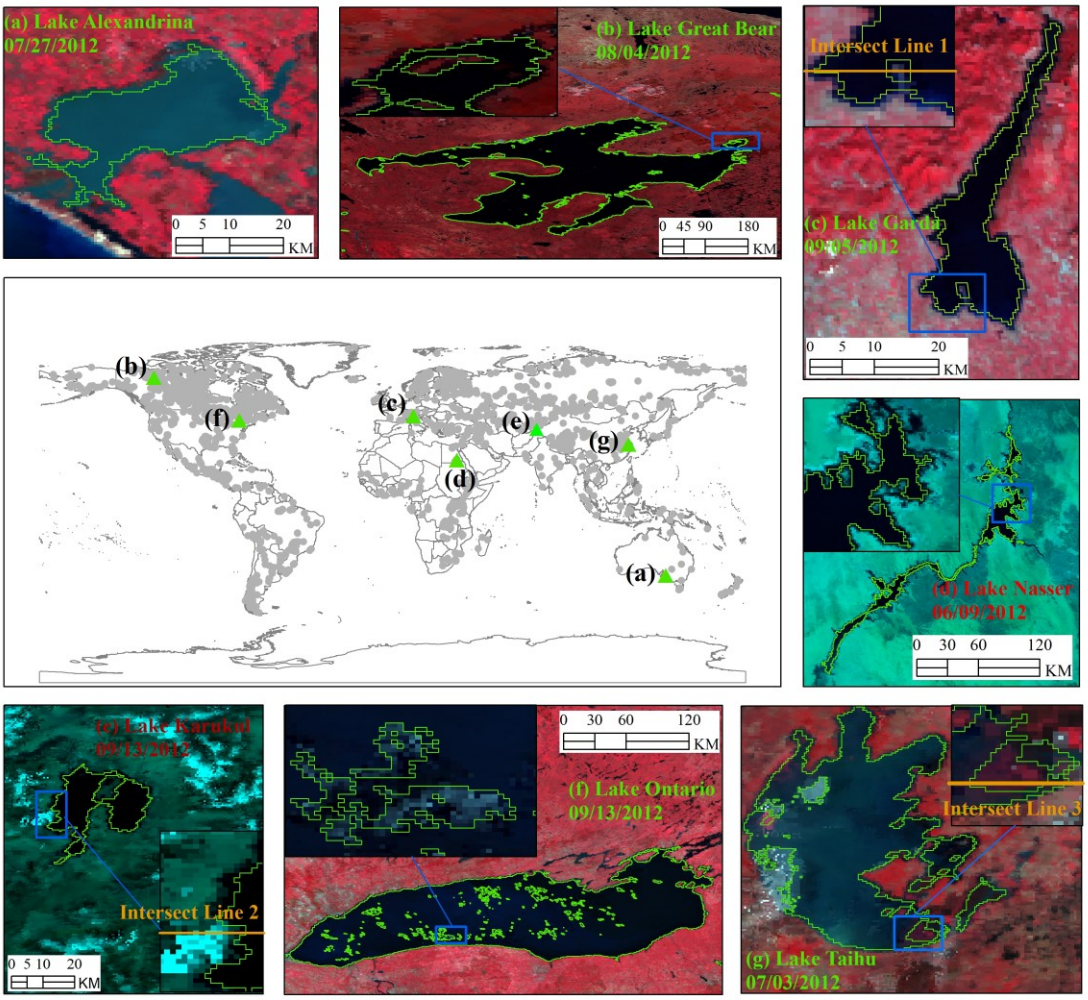

Figure 3 Shorelines of water bodies extracted from MOD09A1 images using the modified histogram bimodal method (MHBM). (a) Lake Alexandrina in Australia; (b) Lake Great Bear in North America; (c) Lake Garda in Europe; (d) Lake Nasser in Africa; (e) Lake Karukul in Asia; (f) Lake Ontario in North America; (g) Lake Taihu in Asia. Green lines denote shorelines. Backgrounds are standard false colour images where red, green, and blue are the 859 nm, 645 nm and 555 nm bands of the MOD09A1 image, respectively. The image acquisition date is listed in each subfigure. The $R_{rs}(1640)$ values of the three intersect lines are shown in Figure 4.

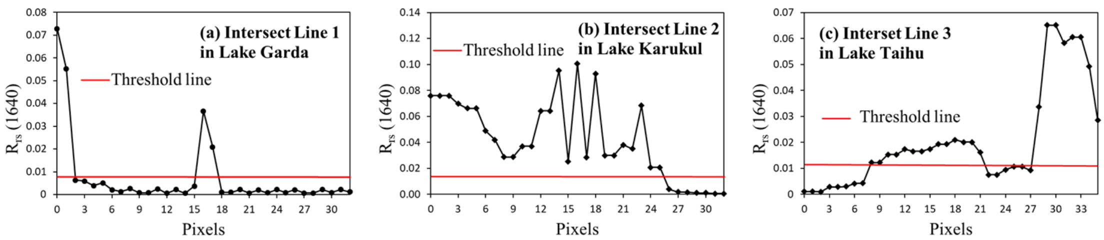

Figure 4 The $R_{rs}(1640)$ values of the intersect lines that marked in Figure 3. (a) Intersect Line 1

through Lake Garda crosses an island inside the lake; (b) Intersect Line 2 through Lake Karukul crosses snow covering the shore side; (c) Intersect Line 3 through Lake Taihu crosses obvious aquatic plants in the water.

3.2.2 Excluding optically shallow water

The extracted water pixels were tested for optically shallow water. Even though optically shallow water for large inland waters (>25 km^2) is seldom found once the identified wetlands in GLWD database are removed, it is possible that bottom reflectance may influence observed water colour, for example in arid or semi-arid saline lakes. Numerous radiative transfer models have been developed that account for the effects of the bottom reflectance and water column on remotely sensed $R_{rs}(\lambda)$ (Lyzenga, 1978; Philpot, 1989; Maritorena et al., 1994; Lee et al., 1998; Mobley and Sundman, 2003). The response types of $R_{rs}(\lambda)$ spectral curves differ with changes in bottom status, water depth, and optical properties of the water (Holden and LeDrew, 2002; Ma et al., 2014; Lee et al., 1998； Lim et al., 2009), and there is no single method that can accurately detect optically shallow water in lakes at the global scale.

To address these challenges, a three-stage method combining automatic identification with manual-intervention was used to identify the optically shallow water bodies:

(1) The MODIS SWIR band (1640 nm) threshold method was adopted in water area segmentation, so that shallow waters with benthic aquatic plants were eliminated from water area due to the higher reflectance in the SWIR band from the aquatic plant that would not be presented in deeper waters (Li et al., 2009);

(2) The blue band threshold method was used as a preliminary means for identifying shallow waters containing a signal from highly reflective sand and sediment bottoms (Lim et al., 2009; Mobley and Sundman, 2003). The threshold (R_{rs}(469 nm) = 0.015 sr^{-1}) was determined by collecting and comparing a large number of $R_{rs}(\lambda)$ spectra of optically shallow and deep waters derived from MOD09A1 images in the summer of 2012 (Figure 5);

(3) Shallow water bodies identified in the first two steps were reviewed using Google Earth and relevant publications (Williams, 2002; Hurlbert, 2012), to remove lakes and reservoirs characterized by deep waters.

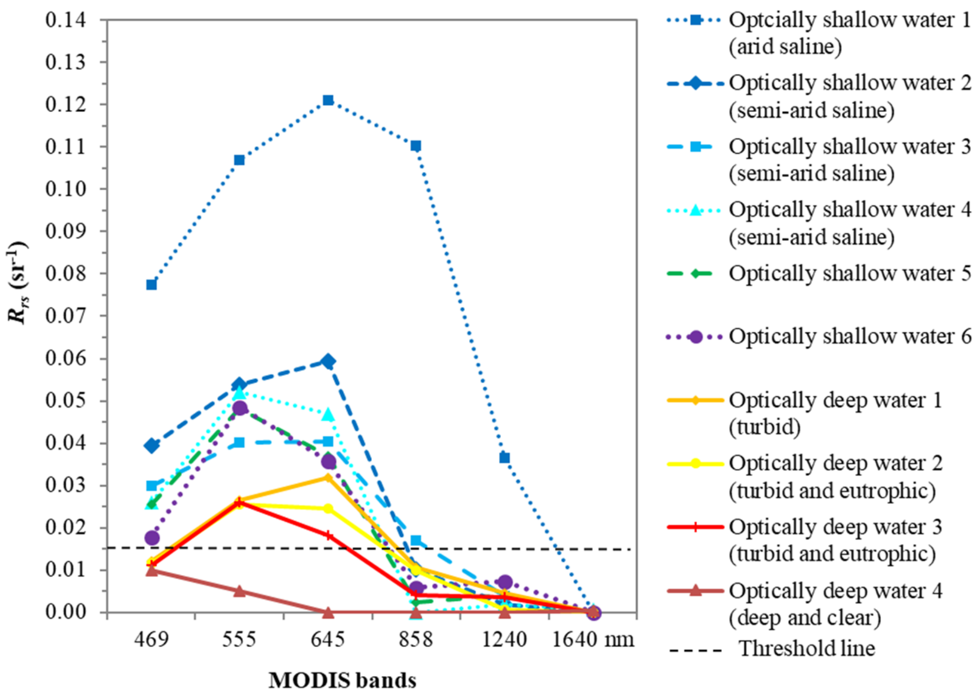

Figure 5 Typical water-leaving reflectance ($R_{rs}(\lambda)$) spectra of optically shallow waters and optically deep waters derived from MOD09A1 images in the summer of 2012. The optically shallow waters 1-4 are Lake Beihuo Luxun, Lake Manas, Lake Margai Caka, and Lake Gasi Kule from Northwest China, and they were described as arid and semi-arid saline lakes in Wang and Dou (1998). The identified optically shallow waters 5 and 6 are Lake George in Australia (Fitzsimmons and Barrows, 2010) and shallow water near the island bank in the Bahamas, respectively (Dierssen et al., 2003);

The dotted line denotes the threshold line (0.015 sr^{-1}) of R_{rs}(469 nm) that used to separate the optically shallow waters.

3.3 FUI retrieval method

In the Commission on Illumination (CIE) colourimetry system, theoretically colour parameters can be calculated from hyperspectral $R_{rs}(\lambda)$ and colour-match functions by using spectral integration in the visible range (C.I.E., 1932; Wang et al., 2015). As there are only three red, green, blue (RGB) bands in MOD09 images (645 nm, 555 nm and 469 nm), the RGB conversion method was used to calculate CIE X, Y, Z using the $R_{rs}(\lambda)$ at the three visible bands (Wang et al., 2015; Li et al., 2016). The RGB conversion equation to X, Y, Z is as follows:

$$\mathrm{X} = 2.7689R + 1{,}7517G + 1.1302B$$

$$\mathrm{Y} = 1.0000R + 4.5707G + 0.0601B$$

$$\mathrm{Z} = 0.0000R + 0.0565G + 5.5934B \tag{3}$$

CIE chromaticity coordinates (x, y) were then calculated from the X, Y, Z by normalizing them to between 0 and 1. A new coordinate system (x', y') was built based on the chromaticity coordinates (x, y) as (Figure 6):

$$\mathrm{x}' = \mathrm{y} - \frac{1}{3}$$

$$\mathrm{y}' = \mathrm{x} - \frac{1}{3} \tag{4}$$

Based on the coordinates (x', y') in the CIE chromaticity diagram, angle α was calculated, defined as the angle between the vector of coordinates (x', y') and the negative x'-axis (at y = 1/3) in the new coordinate system. It is notable that angle α is basically consistent with the definition reported in Wang et al. (2015); but for the convenience of subsequent calculation, starting from the negative x'-axis, the angle α is improved to remain positive now from 0° to 360°. Due to the band setting of satellite sensors, there is a difference between the human eye sensed true colour and the sensor derived colour (Van der Woerd and Wernand, 2015). To eliminate the colour difference caused by MODIS band setting, a systematic deviation delta, defined as the difference between angle α derived from hyperspectral $R_{rs}(\lambda)$ and the equivalent MODIS bands, was modelled and calculated. Following the method presented in Van der Woerd and Wernand (2015), the delta for MODIS was modelled with a polynomial fitting (Figure 7) based on the simulated dataset generated by Hydrolight (IOCCG, 2006). With this delta correction, the angle α and the FUI can be transferable between satellites and sensors with different spectral settings (Van der Woerd and Wernand, 2015). Finally, based on angle α after delta correction, the FUI was calculated using the 21-class FUI lookup table established from the chromaticity coordinates of the Forel-Ule scales (Novoa et al., 2013, Figure 6).

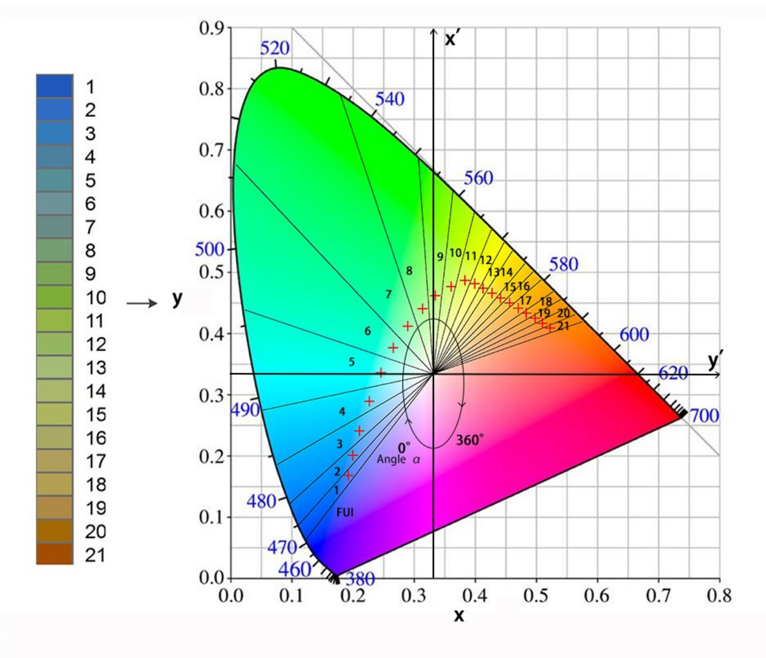

Figure 6 The FUI colours and the subdivision of the FUI from 1 to 21in the CIE chromaticity diagram. The red crosses mark the chromaticity coordinates of the Forel-Ule scales (Novoa et al., 2013). Angle α is the angle between the vector to a point and the negative x'-axis (at y = 1/3).

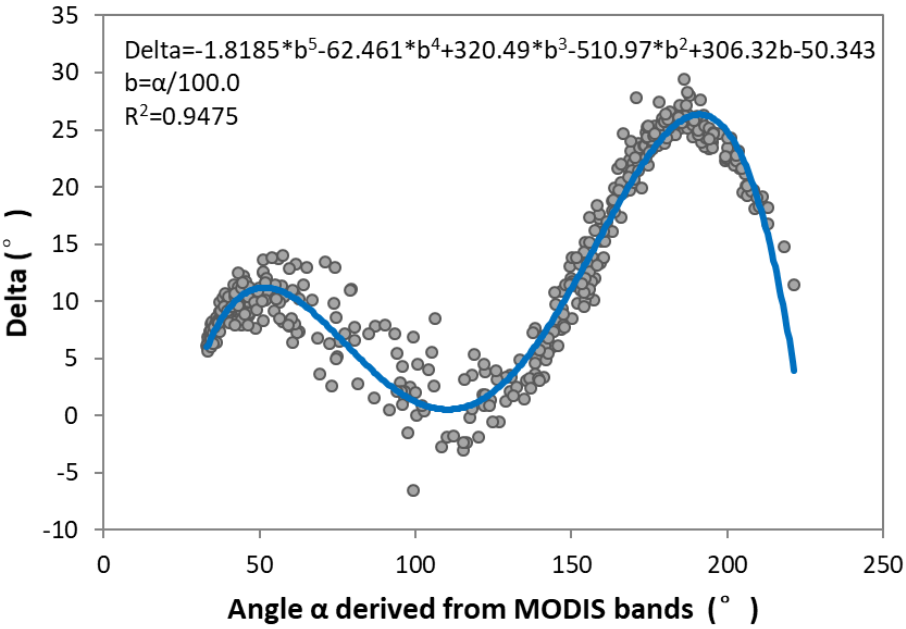

Figure 7 Deviation delta (°) from the hyperspectral angle α as a function of MODIS derived angle α for 0° < α < 230° (i.e., FUI ranging from 1 to 20)

3.4 FUI-based trophic state assessment algorithm

Calculations of the FUI and TSI were initially derived from the Hydrolight simulated dataset to build the theoretical relationship between the two quantities in relatively clear Chl-a dominated waters (Figure 8). Values for TSI ranged from 0 to 68, the FUI generally increased with TSI based on the simulated dataset ($R^2 = 0.94$, N = 500).

However, the relationship between FUI and TSI from the in-situ dataset (Table 1) showed a unimodal distribution (Figure 9): (i) similar to the simulated dataset, when FUI < 10, it increased with TSI ($R^2 = 0.633$), showing that when water colour changes from blue to green, the water body changes from oligotrophic to mesotrophic; (ii) TSI peaked when FUI approached 10, because highly eutrophic waters generally appear green owing to high Chl-a content; (iii) when FUI > 10, it showed a scattered negative relationship with TSI ($R^2 = 0.112$), reflecting the shift from green to brown associated with turbid eutrophic, or humic waters. Based on the in-situ dataset, the relationship for FUI >10 is scattered and loose (Figure 9) because of complex constituents varying independently in turbid waters, but this occasion is underrepresented in the simulated dataset in Figure 8.

Although there are insufficient oligotrophic and mesotrophic waters in the in-situ dataset, the in-situ dataset in Figure 9 showed a roughly similar overall trend as the simulated dataset in Figure 8, and presented the FUI ranges for different trophic states. The dataset showed that 82.7% of in-situ data points with FUI values ≥ 10 were eutrophic with TSI ≥ 50; 83.3% of points with 7 ≤ FUI < 10 (i.e., 10 points out of 12) were mesotrophic while the other two points had TSI values of 29.5 and 50.5. Finally, data points with FUI < 7, were classified as oligotrophic, which is supported by the simulated dataset. The FUI ranges were consequently used to classify the trophic state of the waters.

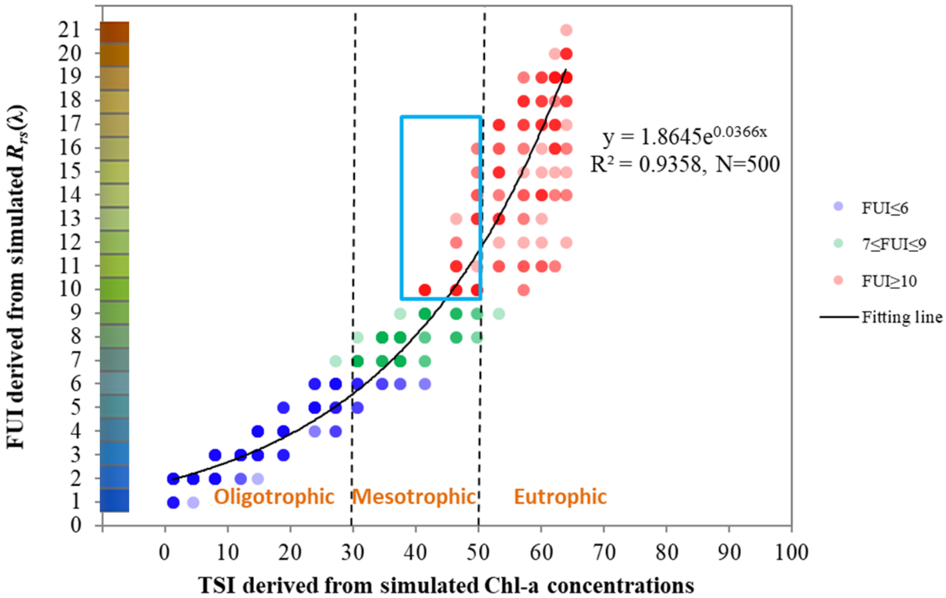

Figure 8 Scatterplot of data pairs of the Forel-Ule index (FUI) and Chl-a-based trophic state index (TSI) from the Hydrolight simulated dataset (N = 500) (IOCCG, 2006). The colour bar indicates the colour of the FUI indices. This simulated dataset covers a wide range of natural waters with concentrations of Chl-a from 0.03 to 30.0 μg/L . The points were plotted with 60% transparency to show the data density. The cyan box marks the mesotrophic points with FUI ≥ 10.

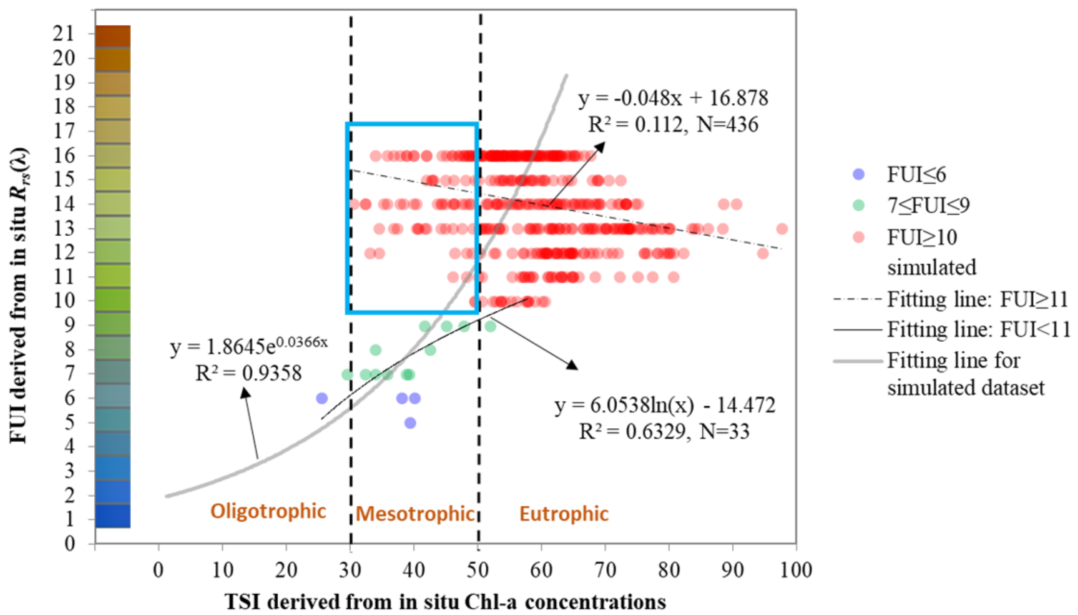

Figure 9 Scatterplot of data pairs of the Forel-Ule index (FUI) and concurrent Chl-a-based trophic state index (TSI) from in-situ measurements (N = 469). The colour bar indicates the colour of the FUI indices. Blue points denote FUI ≤ 6, green spots denote 7 ≤ FUI ≤ 9, and red spots denote FUI ≥ 10. The spots were plotted with 60% transparency to show the density of observations. The cyan box marks the mesotrophic points with FUI ≥ 10.

Some humic (i.e., high CDOM content) or turbid (i.e., high TSM content) mesotrophic waters may result in an FUI value greater than 10 with green to brown colour, such as the scattered points presented in the cyan box in Figure 8 and Figure 9. To distinguish these points, a red band ($R_{rs}(645)$) threshold method was implemented by comparing the $R_{rs}(\lambda)$ spectra of these points with representative $R_{rs}(\lambda)$ spectra of eutrophic waters. Even if water bodies with high CDOM but low TSM appear with a high colour index, $R_{rs}(645)$ will be relatively low compared with other TSM-dominated yellow waters due to low backscattering of the water constituents with high CDOM and low TSM. After applying this threshold, the accuracy of eutrophic classification was increased to 86.8%. With the FUI subsection and the $R_{rs}(645)$ threshold, a decision tree of trophic state assessment for water bodies was developed, shown in Figure 10.

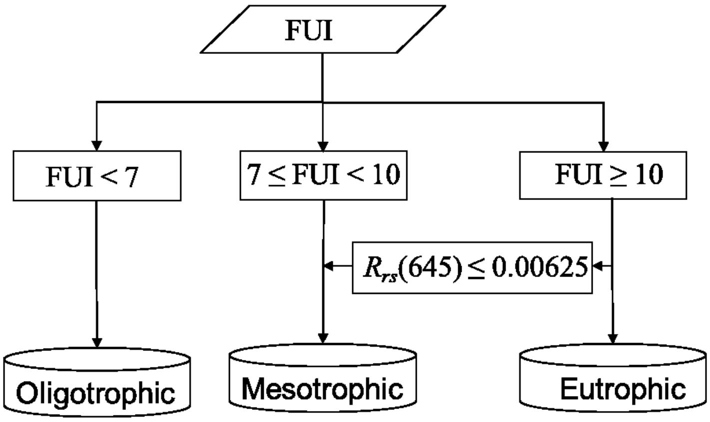

Figure 10 Forel-Ule index (FUI)-based water trophic state assessment decision tree based on the classification of FUI and $R_{rs}(645)$

Lake-average values were considered more appropriate for global applications of the method. Results showed a positive relationship between lake-average FUI and lake-average TSI. For the 10 lakes sampled during 14 field campaigns, only 1 pair of FUI/TSI averages was misclassified based on the FUI from the 10-lake in-situ dataset, supporting the applicability of the method to lake averages.

3.5 Spatial and Temporal statistics

As MOD09A1 is an 8-day composite product, there are globally 16 periods of MOD09A1 images over the four summer months. The seasonal average FUI for each study lake was estimated and used to assess the trophic state of lakes in the summer of 2012. During the calculation, a standard water mask image was produced for each lake by overlaying the water mask images in the same MODIS tile. This was used to check the percentage of noise pixels covered by clouds, ice, snow, and other noises. If the detected water pixels for a lake in an image was less than 30% of its standard water mask area, then those pixels were not considered to represent the entire lake and the image was not used for lake assessment. If less than 3 of the 16 images were valid for a lake over the summer months, then the lake was not assessed in this study. A water body spanning more than one tile of the MOD09A1 image was merged into a single lake by detecting the connected area in the standard water mask images across tiles. To show the variations within each lake, the spatial coefficient of variation (CV = δ/μ, where δ is the standard deviation and μ is the mean) of the FUI and the temporal coefficient of variation for each study lake was also calculated. The average $R_{rs}(645)$ for each lake was computed to aid the FUI-based trophic state assessment.

4. Results

4.1 Evaluation of MODIS retrieved FUI

The FUI values derived from MOD09 $R_{rs}(\lambda)$ and concurrent in-situ $R_{rs}(\lambda)$ were compared to evaluate the FUI retrieved from MODIS with the water-leaving reflectance correction. Despite a few scattered points (with light red colour in Figure 11(a)) that may be caused by the complex atmospheric conditions (e.g. land aerosols), the paired data from the seven lakes showed a strong correlation that mostly fell along the approximate 1:1 line (Figure 11; R^2 = 0.87, slope = 0.92), with a mean absolute difference (MAD) of 0.85 and a mean relative difference (MRD) of 7.5%. In addition, the MODIS FUI produced a 10.5% difference in trophic state classification, compared with the FUI derived from in-situ $R_{rs}(\lambda)$. The effects of various aerosol and solar/viewing geometry perturbations on the FUI calculation are discussed in Section 5.1.

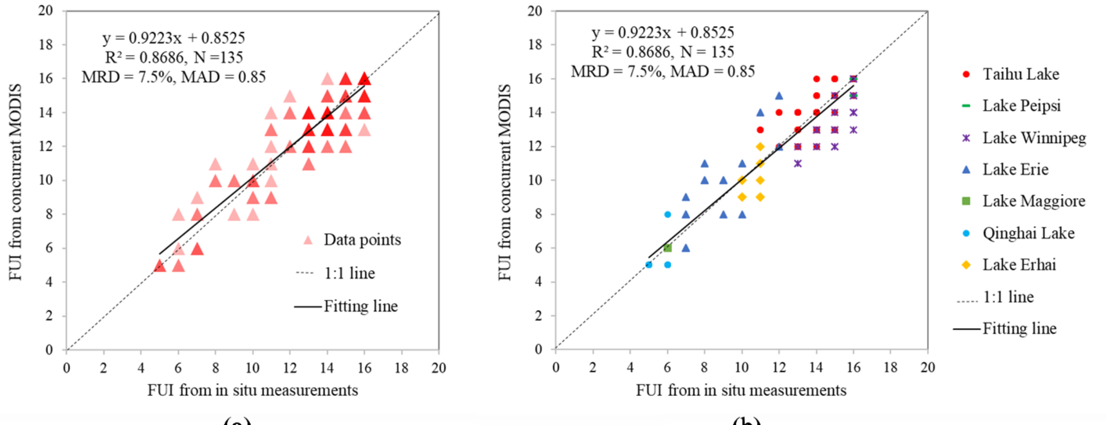

[redacted]

Figure 11 Scatterplots of the FUI derived from in-situ measured $R_{rs}(\lambda)$ versus concurrent MOD09 retrieved $R_{rs}(\lambda)$ for seven lakes with different FUI ranges. (a) Data points are coloured with 60% transparency; darker spots indicate a higher data density. (b) Data points from different lakes are marked with different symbols.

4.2 Validation results with independent data

The lake trophic state data included in the independent validation dataset, as well as the sources of the trophic states data, are listed in Table S1 in Supplementary Material. We found that 20 of the 100 water bodies were misclassified using the FUI-based method. There were no misclassifications between eutrophic and oligotrophic water bodies. Most misclassifications occurred between eutrophic and mesotrophic water bodies, and to a lesser extent between mesotrophic and oligotrophic water bodies. The user accuracy of the oligotrophic, mesotrophic, and eutrophic classifications was 100.0%, 66.7%, and 78.3%, respectively, calculated through confusion matrix analysis. The overall accuracy of the trophic state assessment was found to be 80.0% ($R^2 = 0.75$), while the Kappa coefficient (Landis and Koch, 1977) was 0.67 (Table 2), which confirmed that the FUI-based results were substantially consistent with the comparison dataset.

Table 2 Confusion matrix of Forel-Ule index (FUI)-based trophic state assessment for the investigated 100 lakes

FUI-based Assessment \ Comparison Data	Oligotrophic	Mesotrophic	Eutrophic	Total	User accuracy
Oligotrophic	19	0	0	19	100.0%
Mesotrophic	5	14	2	21	66.7%
Eutrophic	0	13	47	63	78.3%
Total	24	27	49	100	
Producer accuracy	79.2%	51.9%	95.5%		
Kappa coefficient	0.67				
Overall accuracy	80.0%				

4.3 Trophic state assessment for global inland waters in 2012

Among the water bodies studied (N = 2058, total surface area = 1.73 million km^2), the MODIS FUI of the lakes in the summer of 2012 ranged from 2.0 to 17.0, the spatial CV of the water bodies ranged from 0.0% to 41.2% with an average value of 12.9% and the temporal CV ranged from 0.0% to 54.3% with an average value of 9.9%. The season-averaged FUI values of the studied large lakes were found to vary between 3.1 and 16.0, and the mean FUI was 11.1 with a worldwide CV of 26.6% (Figure 12). Based on these data, the results presented that large lake trophic states were not equally distributed around the globe, shown in Figure 13. Eutrophic water bodies accounted for 63.1% of the total number but only 30.5% of the total surface area, mesotrophic water bodies accounted for 26.2% of the total number and 39.4% of the total surface area, and oligotrophic water bodies accounted for 10.7% of the total number but 30.1% of the total surface area.

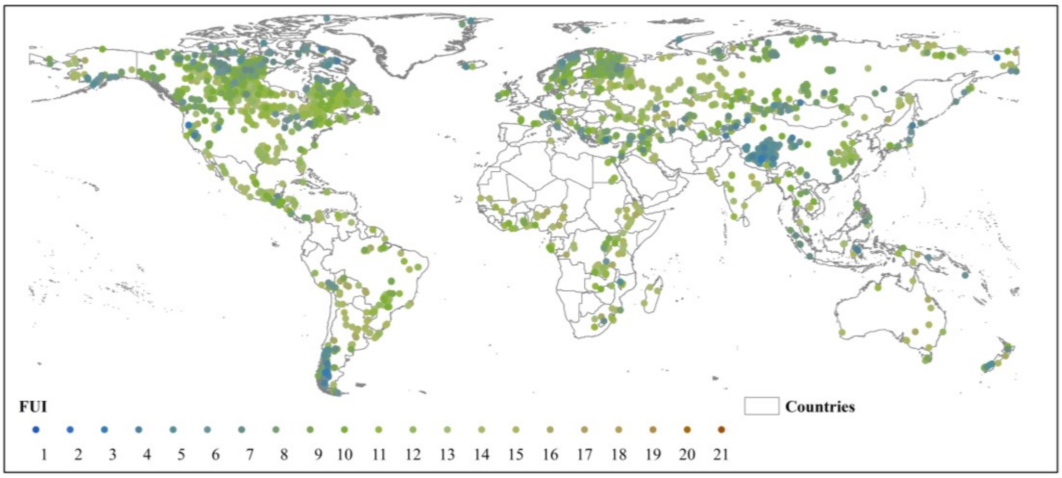

Figure 12 MODIS FUI values for global inland waters in the austral and boreal summers of 2012. Each point represents a single water body of > 25 km^2 in surface area. The FUI of each point represents averaged values from all lake pixels across the summer months rounded to the nearest integer.

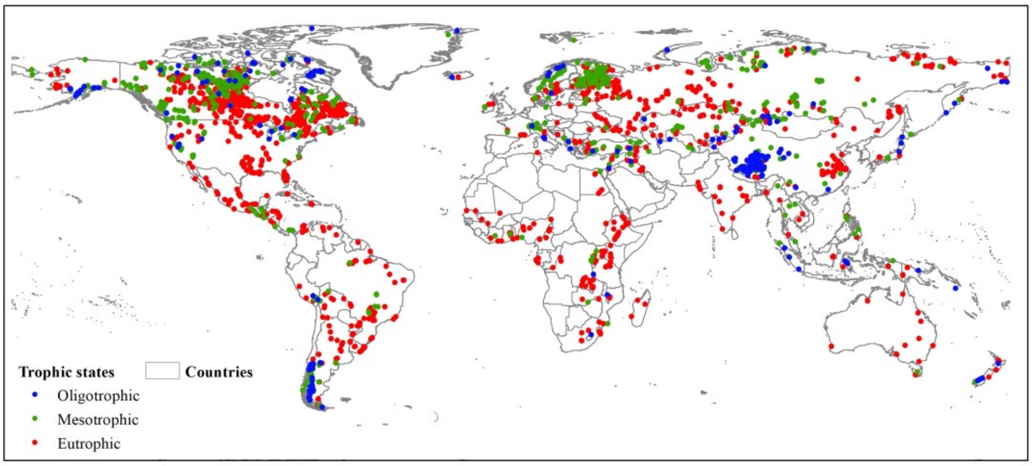

Figure 13 Trophic state classification of global inland waters in the austral and boreal summers of 2012 assessed using the FUI-based method. Blue spots denote oligotrophic water bodies, green spots denote mesotrophic water bodies, and red spots denote eutrophic water bodies.

It was found that oligotrophic large lakes concentrated in high mountains and plateau regions of Central Asia (Qinghai-Tibet Plateau region) and southern South America (Patagonia Plateau region), while eutrophic large lakes concentrated in central

Africa, eastern Asia (East China), and mid-northern and southeast North America (south Canada and southeast U.S.). In terms of lake numbers, Oceania had the highest proportion of oligotrophic large lakes (23.1%), Europe had the highest proportion of mesotrophic large lakes (35.2%), and Africa had the highest proportion of eutrophic large lakes (88.8%). In terms of surface area, North America had the highest proportion of oligotrophic water (49.8%), Asia had the highest proportion of mesotrophic water (71.2%), and Africa still had the highest proportion of eutrophic water (Figure 14).

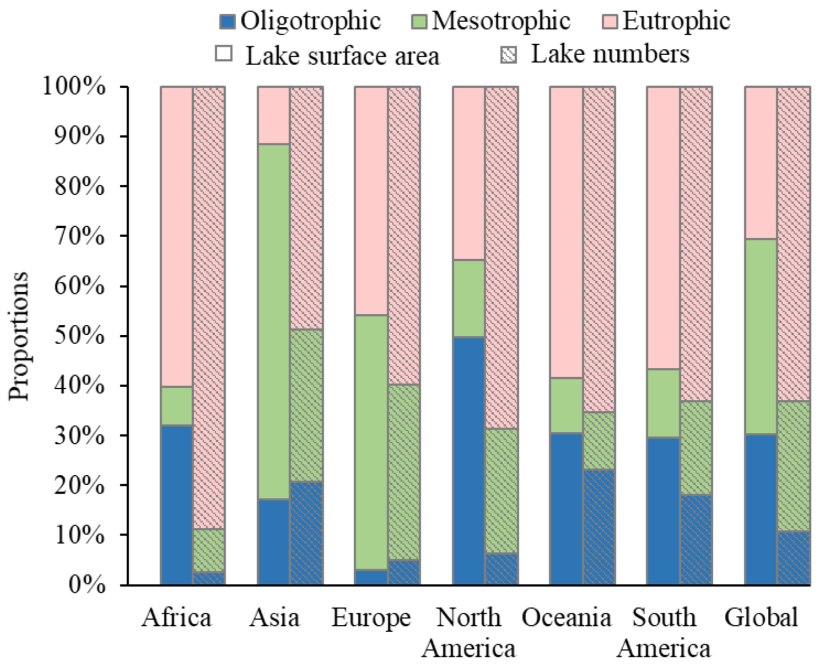

Figure 14 Proportion of large lakes with each trophic state in terms of lake number and lake surface area across continents.

4.4 Trophic state assessment for regional groups of lakes

To further validate the FUI-based trophic state results, data from five regional groups of lakes around the world were analyzed (Figure 15): the North America Great Lakes region (oligo-mesotrophic dominated), the African Great Lakes region (mesotrophic dominated), the central south European region (mesotrophic dominated), the east Asian middle-lower Yangtze region (eutrophic dominated), and the Tibet Plateau (oligotrophic dominated).

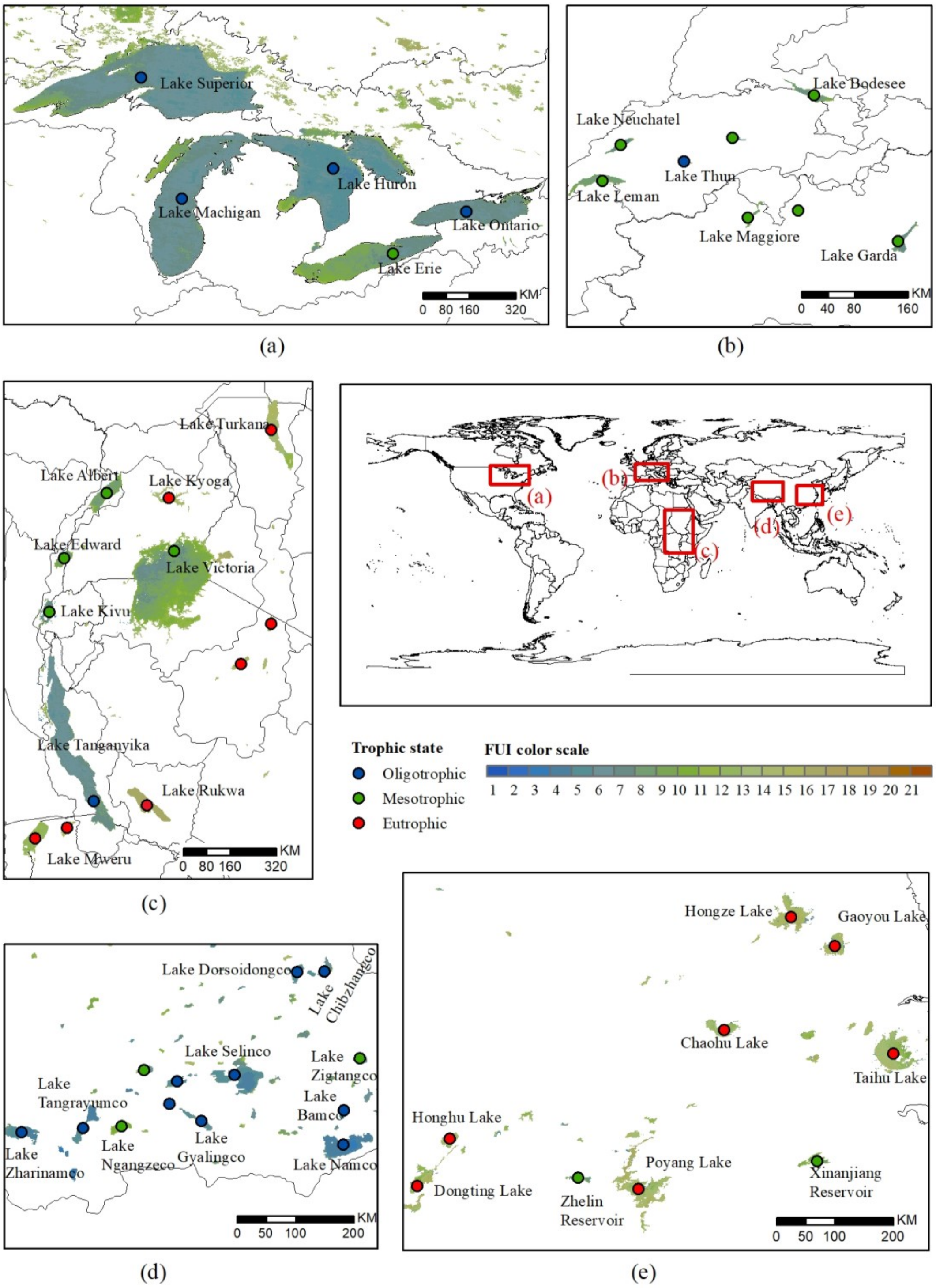

Figure 15 Trophic states and Forel-Ule index (FUI) values of large lakes within typical lake regions in the austral and boreal summers of 2012: (a) North America Great Lakes region; (b) central south European; (c) African Great Lakes region; (d) Tibet Plateau; (e) middle-lower Yangtze region. Coloured points represent the mean trophic state of the water body (blue spots denote oligotrophic water bodies, green spots denote mesotrophic water bodies, and red spots denote eutrophic water bodies).

The FUI of lakes in the North America Great Lakes region mainly ranged from 5 to 10, corresponding to a cyan water colour. Lake Superior, Lake Michigan, Lake Ontario and Lake Huron were found to be oligotrophic, while Lake Erie was found to be mesotrophic. The water colour of western Lake Erie is greener than the other lakes and had an FUI of ~11 (i.e., eutrophic). These results are consistent with those of past studies (Auer et al., 2004; Barbiero et al., 2012; Bridgeman et al., 2013; Chaffin et al., 2011; Holeck et al., 2015; Mukherjee et al., 2016; Shuchman, 2013).

The FUI of lakes in the central south European region mainly ranged from 7 to 9, corresponding to a cyan water colour and a mesotrophic state. This is consistent with past studies, which have classified water bodies in this region as oligo-mesotrophic (Coci, et al., 2015; Rimet et al., 2015; Fuentes et al., 2013; Giardino et al., 2014; Jaquet, 2013; Stich and Brinker, 2010; Vollenweider and Kerekes, 1982).

The FUI of lakes in the African Great Lakes region, which constitutes part of the Rift Valley and East African Rift, mainly varied from 4 to 16, corresponding to a water colour of cyan to green and a wide range of trophic states (oligotrophic, mesotrophic, and eutrophic). Lake Victoria, the second largest freshwater lake in the world, is mesotrophic with eutrophic sections. Lake Turkana, one of the largest desert lakes in the world and the most important regional source of fish, is eutrophic. Lake Tanganyika, the deepest lake in Africa, is oligotrophic. These results are consistent with the past studies (Hecky et al., 2010; Okullo et al., 2011; Avery, 2012; Velpuri et al., 2012; O'Reilly, 2003; Verburg, 2006).

The FUI of lakes on the Tibet Plateau ranged from 2 to 7, corresponding to a water colour of blue to cyan and trophic states that are mainly oligotrophic. Lake Namco, which lies at an elevation of 4718 m and experiences low impact from human activity (Wang and Dou, 1998), was shown to have a very low FUI (2–4) and be oligotrophic. Compared with Lake Namco, the FUI of Lake Selinco was higher (4–7), and its trophic state was oligotrophic but approaching mesotrophic (Li et al., 2016). The FUI of Lake Ngangzeco and Lake Zigtangco were found to be even higher and their trophic states were mesotrophic. Few studies have been implemented for the water trophic states on the Tibet Plateau due to the poor weather conditions. The results in Figure 15 (d) can fill the knowledge gap in this region.

The FUI of the lakes in the middle-lower Yangtze region mainly ranged from 9 to 14, corresponding to a water colour of green to yellow-green, and the trophic states were mainly eutrophic. This is consistent with past studies, which have demonstrated that Lake Taihu, Lake Chaohu, Lake Poyang, and Lake Dongting are typical eutrophic and turbid lakes in China (Chen et al., 2013a, 2013b; Shi et al., 2015; Wang et al., 2011;

Wu et al., 2013; Yang et al., 2013). The trophic states of the Xin'anjiang and Zhelin reservoirs, the two largest reservoirs on the middle-lower reach of the Yangtze, were found to be mesotrophic, which agrees with the results of published literature (Chen, 2009; Sheng et al., 2015).

5. Discussion

5.1 FUI sensitivity to aerosol perturbations and observation conditions

The significant positive correlation between the concurrent FUIs over a wide range of lakes, and the relatively low uncertainties suggest that MODIS surface reflectance data and the water-leaving correction method can be used for FUI retrieval and the FUI-based trophic state assessment of water bodies. Moreover, it is notable that in comparison with concurrent in-situ data (Figure 11), the accuracy of the MODIS FUI (~90%) was greater than that of MODIS $R_{rs}(\lambda)$ (Wang et al., 2016), indicating that the FUI calculation process can reduce uncertainties introduced in MODIS $R_{rs}(\lambda)$.

However, the MOD09 $R_{rs}(\lambda)$ retrieved still theoretically contains some of the uncertainties induced by the effects of aerosol types and bidirectional properties as a result of the MOD09 data and the water-leaving correction method. Hence, the sensitivities of FUI to these uncertainties within the input data were investigated using radiative transfer model simulations. These simulations verified the general global applicability of FUI calculated with this method.

Based on the radiative transfer theory and assuming a non-coupling water-atmosphere system, Rayleigh-corrected reflectance (R_{rc}) can be expressed as:

$$R_{rc}(\lambda) = \rho_t(\lambda) - \rho_r(\lambda) = \rho_a(\lambda) + \pi t(\lambda) t_0(\lambda) R_{rs}(\lambda) \tag{5}$$

where $\rho_t(\lambda)$ is the top-of atmosphere (TOA) reflectance, $\rho_r(\lambda)$ is the reflectance due to Rayleigh scattering, $\rho_a(\lambda)$ is the aerosol reflectance including that from aerosol scattering and aerosol-Rayleigh interactions, $t\,(\lambda)$ is the atmospheric transmittance from the target to the satellite sensor, and $t_0(\lambda)$ is the atmospheric transmittance from the Sun to the target. These unknowns can be calculated from SeaDAS LUTs (look-up tables) for variable aerosols and solar/viewing geometry. Thus, the relationship between $R_{rs}(\lambda)$ and the $R_{rc}(\lambda)$ containing various aerosols can be established through simulations. To determine whether the FUI is sensitive to the considered perturbations, the FUI calculated directly from $R_{rc}(\lambda)$ at MODIS RGB bands were compared with the FUI calculated from the corresponding $R_{rs}(\lambda)$ with the same band setting.

Figure 16 shows the comparison results for maritime and coastal aerosols at the scene center and scene edge. The overall relationship between R_{rs}-based FUI and R_{rc}-based FUI under all light conditions is quite robust ($R^2 = 0.967$) with an MRD of 10.9%, even though the relationship deteriorates a little under coastal aerosols with larger aerosol optical thickness at 869 nm ($\tau(869)$) towards the scene edge. These perturbations resulted in 9.5% of the data indicating a different trophic state to that indicated by the FUI calculated from the original $R_{rs}(\lambda)$ data. The results illustrate that the FUI algorithm is generally insensitive to perturbations due to aerosols and observation conditions. This may be because of the normalization process in the chromaticity coordinate calculation and the clustering process in the 21-indices classification, which may reduce the uncertainties caused by different aerosol types.

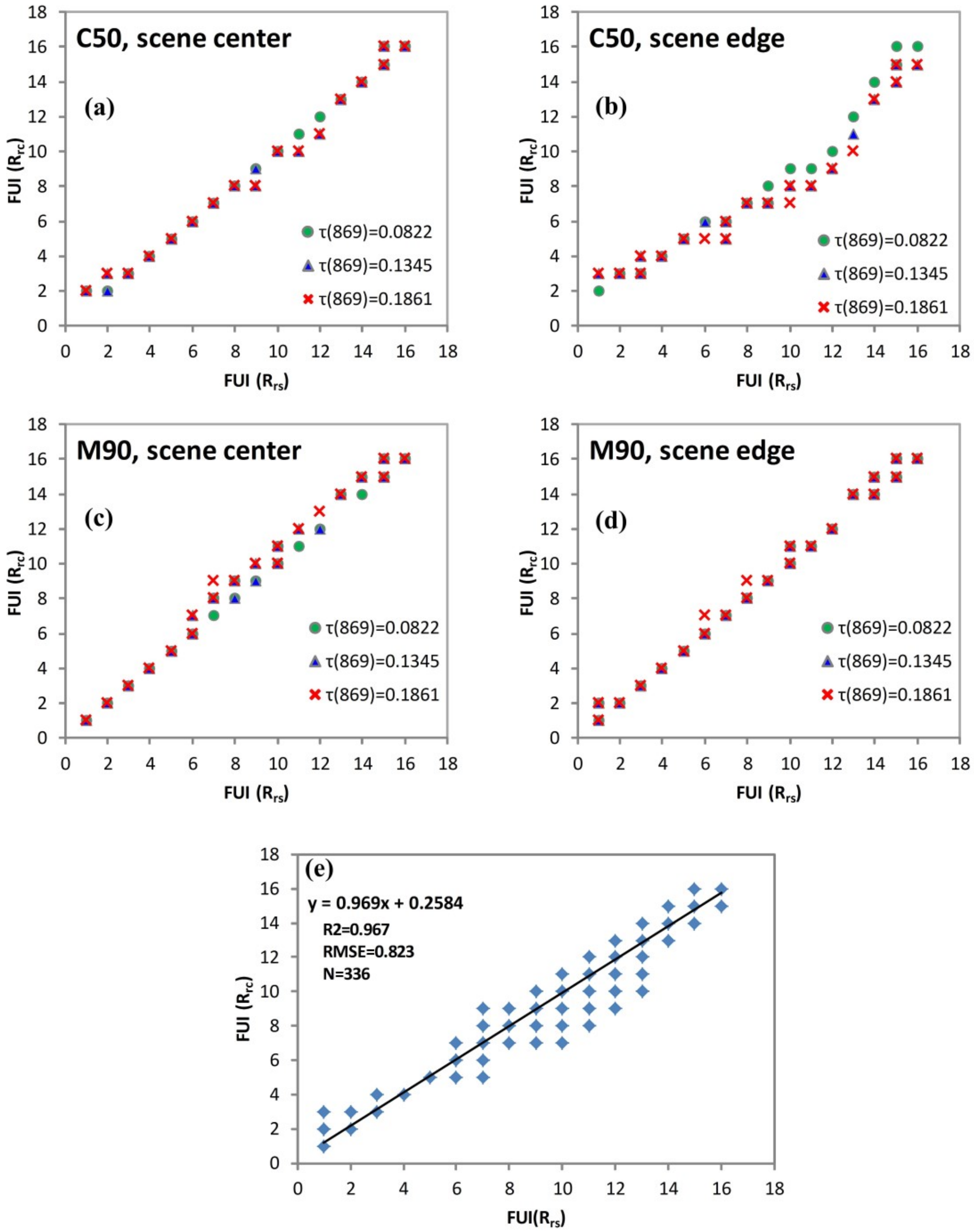

Figure 16 Relationship between R_{rc}-based FUI and R_{rs}-based FUI with various atmospheric conditions (i.e., aerosol type and optical thickness at 869 nm (τ(869))) and solar/viewing geometry, based on model simulations. Two aerosol types were used in the simulations: (a and b) coastal

aerosol with 50% relative humidity (C50) and (c and d) maritime aerosol with 90% relative humidity (M90). Two solar/viewing geometries were performed in the simulations: (a and c) near scene center and (b and d) near scene edge. (e) Relationship between R_{rs}-based FUI and R_{rc}-based FUI under all considered conditions ($R^2 = 0.967$, MRD = 10.9%, RMSD = 0.823, n = 336). MRD denotes the mean relative difference and RMSD denotes the root mean square difference.

5.2 Relationship between the FUI-based method and traditional trophic state assessments

Our FUI-based trophic state assessment method depends on water colour information derived from satellite imagery, which is in contrast to traditional assessment methods that depend on one or several biophysical variables (i.e., Chl-a, SD, TP, TN, COD and biomass; Burns et al., 1999; Vant, 1987). To compare the FUI-based method with traditional variables, we compared our results with data in the NLA2007 report (USEPA, 2009), which contains both Chl-a based trophic state assessments, and additional trophic state assessments based on SD, TP, and TN. Using the 20 lakes found in both datasets, the results showed that the FUI-based classifications were better correlated with SD and Chl-a ($R^2 = 0.80$, 0.65, $p < 0.05$, RD (relative error) = 30%; Figure 17), reflecting the importance of water clarity and Chl-a in controlling water colour. The correlation between the FUI-based results and TP-based trophic state assessments was also strong ($R^2 = 0.29$, $p < 0.05$, RD = 35%). However, the TN-based results had a weak relationship with the FUI-based results ($R^2 = 0.03$, RD = 55%). Similarly, the TN-based results had an insignificant relationship with the Chl-a-based results ($R^2 = 0.03$), as there is usually a weak relationship between TN and Chl-a in lakes (Guildford and Hecky, 2000).

Of the 20 U.S. lakes compared, none were classified as oligotrophic in the FUI-based results (Figure 17), but 5 lakes were classified as oligotrophic in the Chl-a-based NLA results. This misclassification of oligotrophic lakes as mesotrophic was also seen in the validation comparison data (Table 2), which will be discussed in Section 5.3.

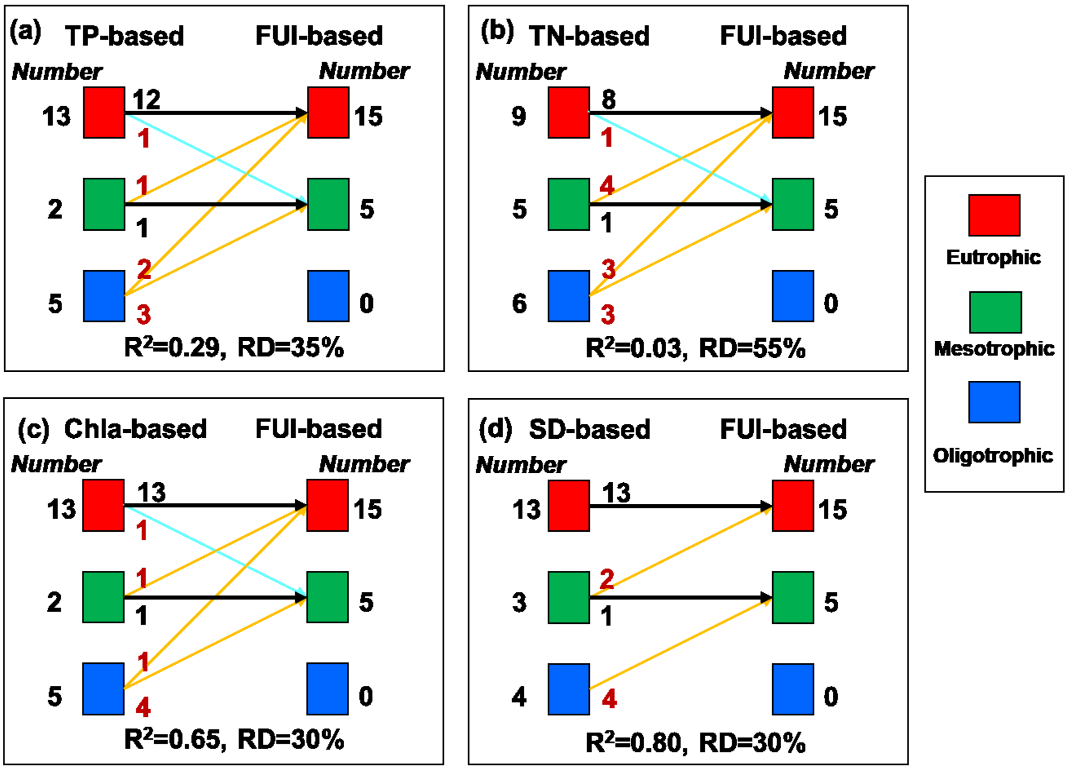

Figure 17 Comparison of lakes classified as different trophic states using the Forel-Ule index (FUI)-based trophic state results and National Lake Assessment 2007 (USEPA, 2009) results based on (a) total phosphorus (TP), (b) total nitrogen (TN), (c) chlorophyll-a (Chl-a), and (d) Secchi depth (SD), for the 20 matched lakes. R^2 denotes the determination coefficient and RD denotes the relative error.

5.3 Uncertainties of trophic state assessment using FUI

Since there is currently no single RS algorithm applicable for the global inland waters to retrieve the trophic state related parameters (i.e.Chl-a), as a relatively easy-to-produce image product, the FUI-based method makes it possible to assess the trophic states of global inland waters. Although the trophic state of the waters across the in-situ dataset and independent dataset could be classified with relatively high accuracy (~80%) with the FUI, the confusion matrix of the FUI-based classification for 100 investigated lakes (Table 2) shows that the FUI method led to an over-estimation of the trophic state of a small proportion of lakes. This may be explained by differences in the division of the trophic states by different different assessing methods. The trophic state classification in this study adopted the boundaries of 1 and 7 μg/L, based on Carlson (1977). However, the USEPA (2016) adopted the boundaries of 2 and 7 μg/L. Hence, there may be some over-estimation in the mesotrophic state when using the FUI method because of the lower boundary. The other reason might be that the FUI of waters may appear larger when there are other optically active constituents in addition to Chl-a that dominate these optically complex inland waters.

We identified the mesotrophic waters from the eutrophic waters with FUI $\geq$ 10 by using a red band (R_{rs}(645)) threshold method, because the relatively high CDOM content in water changes the water colour to green and yellow, and the backscattering of the water in the red band is quite low because of the low TSM content. In the cyan box in Figure 9, there were a few other situations that result in the misclassification of mesotrophic waters, which are shown in Figure 17. For these mesotrophic waters with FUI $\geq$ 10， the optical properties are generally dominated by abundant CDOM or TSM. Mesotrophic water dominated by relatively high CDOM and with very low TSM can be identified from eutrophic water using the red band threshold method. However, for water dominated by high CDOM with relatively high TSM, the $R_{rs}(\lambda)$ spectra is similar to eutrophic waters and cannot be distinguished using the MODIS bands. It is difficult to distinguish between mesotrophic and eutrophic waters when dominated by high TSM with the MODIS imagery. Further assessment of the trophic state of these two specific situations will require platforms with superior spectral resolution.

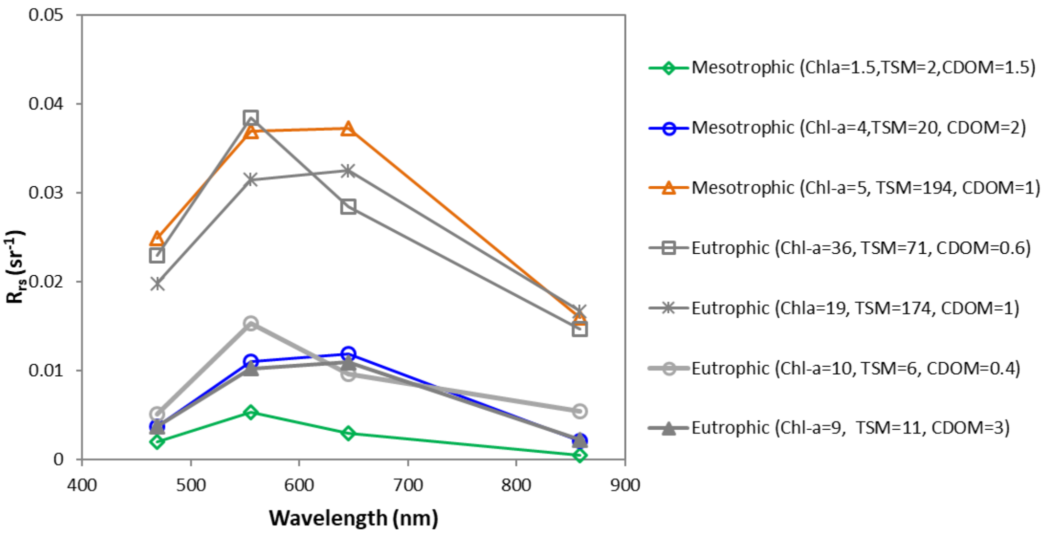

Figure 17 Different types of water-leaving reflectance ($R_{rs}(\lambda)$) spectra of waters with FUI≥10, including eutrophic and confusing mesotrophic waters. The unit for Chl-a is μg/L, for TSM is mg/L, for CDOM is m^{-1} which means the absorption coefficient at 440 nm.

As the summer-average FUI of each water body was used to assess the trophic state of the water body, the averaging processes may result in the loss of spatial and temporal characteristics of some water bodies, whilst reducing the occurrence of unexpected errors and uncertainties. In this case, a water body that is partly eutrophic and partly mesotrophic may be classified as mesotrophic after the averaging process. The timing of the images also affects the results, as the trophic state of lake may change during the summer months. Therefore, a threshold for the number of images of no less than three over the summer months is therefore considered necessary and avoids the cases where two consecutive images may produce a biased result against the average state. From the global results, the spatial CV of the water bodies ranged from 0.0% to 41.2% with an average value of 12.9%, and the temporal CV ranged from 0.0% to 54.3% with an average value of 9.9%. Large variations in these waters might in part be related to the impact of cloud cover influencing or biasing the pixel coverage for a lake for different areas, whilst some may also be related to extreme events such as sudden algae blooms or sediment plumes following heavy rainfall.

The data quality of MODIS Terra was often considered not adequate for ocean colour applications (Franz et al., 2008). But around 2010, NASA started reprocessing of all the MODIS Terra products and produced good agreement with MODIS Aqua by using improved radiometric calibration to account for sensor degradation (Li et al., 2017; Lyapustin et al., 2014; Meister and Franz, 2011). In addition, for inland waters, the water signal has a greater contribution in the TOA radiance, which tends to be much greater than that associated with open ocean waters.

There may be some uncertainties induced by the calibration of Terra MODIS and the artefacts of atmospheric correction in the derivation of $R_{rs}(\lambda)$ and FUI from Terra MOD09 products in this study. Nevertheless, following the simple water-leaving reflectance correction, the comparison between MODIS FUI and in-situ derived FUI and the evaluation of the FUI sensitivity to remaining data perturbations produced good results and demonstrated the validity and practicability of the MOD09 product and the simple correction method for a wide range of inland waters. As might be expected, the producer accuracies (Liu et al., 2007) in the confusion matrix (Table 3) for darker waters like oligotrophic and mesotrophic waters, are relatively low (79.2% and 51.9%). As described, this is likely associated with calibration errors and artefacts introduced from atmospheric correction over dark waters (Wang et al., 2016). Hence, for global inland waters with various optical properties, a more robust atmospheric correction for satellite products remains a high research priority.

Moreover, we chose Terra MOD09 as the main data source rather than Aqua MYD09 because of the frequent stripe noise. The stripe noise in band 6 (1640 nm) is severe in the Aqua MYD09 and Aqua MYD02 (the Level-1B Calibrated Geolocation Data Set), which is induced by the detectors in Aqua MODIS band 6 and has been reported in numerous studies (Rakwatin et al., 2009; Wang et al., 2006; Doelling et al., 2015). Band 6 is a useful SWIR band used in this study to detect water areas and atmospheric noises; however, the stripe noise in this band in Aqua would result in inaccurate water area masks and water-leaving reflectance.

5.4 Applicability to new satellite sensors

The FUI retrieval algorithms from the water-leaving reflectance spectra have been established for various satellite sensors such as MODIS, MERIS, Landsat-8 OLI, Sentinel-3 OLCI (Wang et al., 2015; Wernand et al., 2013; Van der Woerd and Wernand, 2015, 2018). There are two main approaches for calculating CIE tristimulus X, Y, Z. One is to rebuild the spectral data using an interpolation approach (Van der Woerd and Wernand, 2015, 2018). The other approach is specific to sensors with only RGB bands in the visible range, and it converts RGB to CIE X, Y, Z using the conversion equation, as shown in Equation (3) (C.I.E., 1932; Wang et al., 2015). However, despite whether an interpolation approach or the RGB conversion approach is used, there would be colour differences from the human eye sensed true colour caused by the band setting of the sensors (Van der Woerd and Wernand, 2015). To remove this difference, a delta correction method was introduced by Van der Woerd and Wernand (2015) and adopted in this study which models the difference between the sensor results and the true colour results using polynomial fittings. Therefore, with the delta correction, the FUI and the angle α calculated can be comparable and transferable between different satellite sensors (Van der Woerd and Wernand, 2015, 2018). It is notable that the definition for angle α enables it increase with FUI in this study, while the definition for angle α in Van der Woerd and Wernand (2015) results in a decrease with FUI considering the different start and revolving direction of angle α adopted. A transfer is first required when comparing angle α derived using the different definitions. Regardless of the definition of angle α, the FUI calculated are consistent because the same set of chromaticity coordinates of the Forel-Ule scales were used (Novoa et al., 2013). Furthermore, the FUI calculated from new sensors, like Landsat-8 OLI and Sentinel-3

OLCI, could be generally comparable with that from MODIS using a proper correction method for the band settings (Van der Woerd and Wernand, 2018). With recently launched sensors such as the Landsat-8 OLI and Sentinel-2(A & B), smaller lakes can be added to the dataset to achieve more comprehensive global results.

6. Conclusions

In this study, the trophic states of global large inland waters were assessed using an FUI-based remote sensing algorithm. The successful outcome can be attributed to two factors: (1) the water colour index, FUI, can be calculated from MOD09A1 data with considerable accuracy (~90%) through comparison with in-situ data, and it is nearly immune to aerosol perturbations and variations in observation conditions. Such tolerances lead to significantly increased validity, which is critical to FUI's application on the global scale; (2) The FUI-based trophic state assessment algorithm was developed based on the analysis of the relationship between FUI and TSI from 469 samples from in-situ measurements at 10 lakes around the world, which contain a wide range of optical and water quality properties. This led to a robust trophic state assessment method for inland waters on large scales, and an overall accuracy of 80% was achieved. This algorithm could be applied to other satellite sensors with the establishment of FUI retrieval algorithms from various sensors.

The assessment algorithm was implemented on MODIS images collected in the austral and boreal summers of 2012, and the trophic states of the water bodies were classified as oligotrophic, mesotrophic, or eutrophic. Of the 2058 water bodies considered, eutrophic water bodies accounted for 63.1% of the total number but only 30.5% of the total surface area, mesotrophic water bodies accounted for 26.2% of the total number and 39.4% of the total surface area, and oligotrophic water bodies accounted for 10.7% of the total number but 30.1% of the total surface area. Oligotrophic large lakes were found to be concentrated in plateau regions in Central Asia and southern South America, while eutrophic large lakes were concentrated in central Africa, eastern Asia, and mid-northern and southeast North America.

Acknowledgements

This research was sponsored by the National Key Research and Development Program of China (2016YFB0501502), National Natural Science Foundation of China (41325004, 41471308, and 41671203), Youth Innovation Promotion Association of Chinese Academy of Sciences (2015128), and China Scholarship Council. We also gratefully acknowledge the UK NERC GloboLakes project (NE/J024279/1), including the Limnades data base (www.limnades.org). Moritz Lehmann was funded by grant UOWX1503 from the New Zealand Ministry for Business, Innovation and Employment.

References

Auer, M. T., Bub, L. A. (2004). Selected features of the distribution of chlorophyll along the southern shore of Lake Superior. Journal of Great Lakes Research, 30, 269-284.

Avery, S., Eng, C. (2012). Lake Turkana & the Lower Omo: hydrological impacts of major dam and irrigation developments. African Studies Centre, the University of

Oxford.

Baban, S. M. (1996). Trophic classification and ecosystem checking of lakes using remotely sensed information. Hydrological sciences journal, 41(6), 939-957.

Barbiero, R. P., Lesht, B. M., Warren, G. J. (2012). Convergence of trophic state and the lower food web in lakes huron, michigan and superior. Journal of Great Lakes Research, 38(2), 368-380.

Beeton, A. M., Edmondson, W. T. (1972). The eutrophication problem. Journal of the Fisheries Board of Canada, 29(6), 673-682.

Bigham Stephens, D. L., Carlson, R. E., Horsburgh, C. A., Hoyer, M. V., Bachmann, R. W., Canfield Jr, D. E. (2015). Regional distribution of Secchi disk transparency in waters of the United States. Lake and Reservoir Management, 31(1), 55-63.

Binding, C. E., Greenberg, T. A., Watson, S. B., Rastin, S., Gould, J. (2015). Long term water clarity changes in North America's Great Lakes from multi-sensor satellite observations. Limnology and Oceanography, 60(6), 1976-1995. http://doi.org/10.1002/lno.10146.

Binding, C. E., T. A. Greenberg, and R. P. Bukata. (2013). The MERIS Maximum Chlorophyll Index; its merits and limitations for inland water algal bloom monitoring. J. Great Lakes Res. 39: 100–107. doi:10.1016/j.jglr.2013.04.005

Bridgeman, T. B., Chaffin, J. D., Filbrun, J. E. (2013). A novel method for tracking western Lake Erie Microcystis blooms, 2002–2011. Journal of Great Lakes Research, 39(1), 83-89.

Bukata, P. R., Jerome, J. H., Kondratyev, K. Y., Pozdnyakov, D. (1995). Optical Properties and Remote Sensing of Inland and Coastal Waters Boca Raton: CRC Press.

Bukata, R. P., Bruton, J. E., Jerome, J. H. (1983). Use of chromaticity in remote measurements of water-quality. Remote Sensing of Environment, 13(2), 161-177.

Burns, N. M., Bryers, G. (2000). Protocols for monitoring trophic levels of New Zealand lakes and reservoirs. Ministry for the Environment.

Burns, N. M., Rutherford, J. C., Clayton, J. S. (1999). A monitoring and classification system for New Zealand lakes and reservoirs. Lake and Reservoir Management, 15(4), 255-271.

C.I.E. (1932). Commission Internationale de l'Eclairage Proceedings 1931, Cambridge Univ. Press, 19-29.

Carlson, R. E. (1977). A trophic state index for lakes. Limnology and oceanography, 22(2), 361-369.

Carlson, R. E. (1991). Expanding the trophic state concept to identify non-nutrient limited lakes and reservoirs. Enhancing the states's lake management programs, 59-71.

Chaffin, J. D., Bridgeman, T. B., Heckathorn, S. A., Mishra, S. (2011). Assessment of Microcystis growth rate potential and nutrient status across a trophic gradient in western Lake Erie. Journal of Great Lakes Research, 37(1), 92-100.

Chen, J., Quan, W., Zhang, M., Cui, T. (2013a). A simple atmospheric correction algorithm for MODIS in shallow turbid waters: A case study in Taihu Lake. IEEE Journal of Selected Topics in Applied Earth Observations and Remote Sensing, 6(4), 1825-1833.

Chen, L. (2003). A study of applying genetic programming to reservoir trophic state evaluation using remote sensor data. International Journal of Remote Sensing, 24(11), 2265-2275.

Chen, R. (2009). Research on water quality appraisal and water environmental capacity of Zhelin Reservoir. Master Dissertation. Nanchang University.

Chen, X., Yang, X., Dong, X., Liu, E. (2013b). Environmental changes in Chaohu Lake (southeast, China) since the mid-20th century: the interactive impacts of nutrients, hydrology and climate. Limnologica-Ecology and Management of Inland Waters, 43(1), 10-17.

Cheng, K. S., Lei, T. C. (2001). Reservoir trophic state evaluation using Landsat TM images. Journal of the American Water Resources Association, 37, 1321-1334.

Chernetskiy, M., Shevyrnogov, A., Shevnina, S., Vysotskaya, G., Sidko, A. (2009). Investigations of the Krasnoyarsk Reservoir waters based on the multispectral satellite data. Advances in Space Research, 43(2), 206-213.

Coci, M., Odermatt, N., Salcher, M. M., Pernthaler, J., Corno, G. (2015). Ecology and distribution of thaumarchaea in the deep hypolimnion of Lake Maggiore. Archaea-an International Microbiological Journal, 2015.

Diaz, M., Pedrozo, F. and Baccala, N. (2000). Summer classification of Southern Hemisphere temperate lakes (Patagonia, Argentina). Lakes & Reservoirs: Research & Management, 5: 213–229.

Dierssen, H.M., Zimmerman, R.C., Leathers, R.A., Downes, T.V. and Davis, C.O., 2003. Ocean color remote sensing of seagrass and bathymetry in the Bahamas Banks by high - resolution airborne imagery. Limnology and oceanography, 48(1part2), pp.444-455.

Doelling, D. R., Wu, A., Xiong, X., Scarino, B. R., Bhatt, R., Haney, C. O., Gopalan, A. (2015). The radiometric stability and scaling of collection 6 Terra-and Aqua-MODIS VIS, NIR, and SWIR spectral bands. IEEE Transactions on Geoscience and Remote Sensing, 53(8), 4520-4535.

Duan, H., Zhang, Y., Zhang, B., Song, K., Wang, Z. (2007). Assessment of chlorophyll-a concentration and trophic state for Lake Chagan using Landsat TM and field spectral data. Environmental monitoring and assessment, 129(1-3), 295-308.

Fitzsimmons, K. E., Barrows, T. T. (2010). Holocene hydrologic variability in temperate southeastern Australia: an example from Lake George, New South Wales. The Holocene, 20(4), 585-597.

Forsberg, D., Ryding, S. O. (1980). Eutrophication parameters and trophic indices in 30 Swedish lakes. Arch Hydrobiol.89:189–207.

Friedl, M. A., Sulla-Menashe, D., Tan, B., Schneider, A., Ramankutty, N., Sibley, A., andHuang, X. (2010). MODIS Collection 5 global land cover: Algorithm refinements and characterization of new datasets. Remote Sensing of Environment, 114, 168–182.

Fuentes, N., Güde, H., Wessels, M., Straile, D. (2013). Allochthonous contribution to seasonal and spatial variability of organic matter sedimentation in a deep oligotrophic lake (Lake Constance). Limnologica-Ecology and Management of Inland Waters, 43(2), 122-130.

Garaba, S. P., Badewien, T. H., Braun, A., Schulz, A.-C., Zielinski, O. (2014). Using ocean colour remote sensing products to estimate turbidity at the Wadden Sea time series station Spiekeroog. J. Europ. Opt. Soc. Rap. Public. 9 (14020): 1-6.

Giardino, C., Bresciani, M., Stroppiana, D., Oggioni, A., Morabito, G. (2013). Optical remote sensing of lakes: an overview on Lake Maggiore. Journal of Limnology, 73(s1).

Giardino, C., Bresciani, M., Cazzaniga, I., Schenk, K., Rieger, P., Braga, F., et al. (2014). Evaluation of multi-resolution satellite sensors for assessing water quality and bottom depth of lake garda. Sensors, 14(12), 24116-31

Guildford, S.J. and Hecky, R.E., (2000). Total nitrogen, total phosphorus, and nutrient limitation in lakes and oceans: is there a common relationship?. Limnology and Oceanography, 45(6), 1213-1223.

Härmä, P., Vepsäläinen, J., Hannonen, T., Pyhälahti, T., Kämäri, J., Kallio, K. (2001). Detection of water quality using simulated satellite data and semi-empirical algorithms in Finland. Science of the Total Environment, 268(1), 107-121.

Hecky, R. E., Mugidde, R., Ramlal, P. S., Talbot, M. R., Kling, G. W. (2010). Multiple stressors cause rapid ecosystem change in Lake Victoria. Freshwater Biology, 55(s1), 19-42.

Holden, H., LeDrew, E. (2002). Measuring and modeling water column effects on hyperspectral reflectance in a coral reef environment. Remote Sensing of Environment, 81(2), 300-308.

Holeck, K. T., Rudstam, L. G., Watkins, J. M., Luckey, F. J., Lantry, J. R., Lantry, B. F., Johnson, T. B. (2015). Lake Ontario water quality during the 2003 and 2008 intensive field years and comparison with long-term trends. Aquatic Ecosystem Health & Management, 18(1), 7-17.

Hou, X., Feng, L., Duan, H., Chen, X., Sun, D., Shi, K. (2017). Fifteen-year monitoring of the turbidity dynamics in large lakes and reservoirs in the middle and lower basin of the Yangtze River, China. Remote Sensing of Environment, 190, 107-121.

Hu, C., K. L. Carder, and F. E. Muller-Karger. (2000). Atmospheric Correction of SeaWiFS Imagery over Turbid Coastal Waters: A Practical Method. Remote Sensing of Environment 74: 195–206. doi:10.1016/S0034-4257(00)00080-8.

Hu, C., Lee, Z., Ma, R., Yu, K., Li, D., Shang, S. (2010). Moderate resolution imaging spectroradiometer (MODIS) observations of cyanobacteria blooms in Taihu Lake, China. Journal of Geophysical Research: Oceans, 115(C4).

Hurlbert, S. H. (Ed.). (2012). Saline Lakes V: Proceedings of the Vth International Symposium on Inland Saline Lakes, held in Bolivia, 22–29 March 1991 (Vol. 87). Springer Science & Business Media.

IOCCG (2006). Remote sensing of Inherent Optical Properties: fundamentals, tests of algorithms, and applications. Lee, Z.-P. (ed.), Reports of the International Ocean-Colour Coordinating Group, No. 5, IOCCG, Dartmouth, Canada.

Jacobs L L. (1989). Limnological characteristics of big and litile minto lakes, Alaska. Alaska's hidden resource, 1989: 17.

Jaquet, J. M., Nirel, P., Martignier, A. (2013). Preliminary investigations on picoplankton-related precipitation of alkaline-earth metal carbonates in meso-oligotrophic Lake Geneva (Switzerland). Journal of Limnology, 72(3), 50.

Jin, X. C., Tu, Q. Y. (1990). The standard methods for observation and analysis in lake eutrophication. Chinese Environmental Science Press, Beijing, 240.

Jones, R. A., Lee, G. F. (1982). Recent advances in assessing impact of phosphorus loads on eutrophication-related water quality. Water Research, 16(5), 503-515.

Joniak, T., Nagengast, B., Kuczynska-Kippin, N. (2009). Can popular systems of trophic classified be used for small water bodies? Oceanological and hydrobiological studies. International Journal of oceanography and hydrobiology, XXXVIII(4), 145–151

Khandelwal, A., Karpatne, A., Marlier, M. E., Kim, J., Lettenmaier, D. P., Kumar, V. (2017). An approach for global monitoring of surface water extent variations in reservoirs using MODIS data. Remote Sensing of Environment.

Kingston, John. (2015). Completion Report Mille Lacs Lake Paleolimnology Project. http://hdl.handle.net/10792/1832.

Klein, I., Gessner, U., Dietz, A. J., Kuenzer, C. (2017). Global WaterPack–A 250 m resolution dataset revealing the daily dynamics of global inland water bodies. Remote Sensing of Environment, 198, 345-362.

Knight, J. F., Voth, M. L. (2012). Application of MODIS imagery for intra-annual water clarity assessment of Minnesota lakes. Remote Sensing, 4(7), 2181-2198.

Kshitij Mishra and P. Rama Chandra Prasad. (2015). Automatic extraction of water bodies from Landsat imagery using Perceptron model, Journal of Computational Environmental Sciences, vol. 2015, Article ID 903465, 9 pages, 2015. doi:10.1155/2015/903465

Kutser, T., E. Vahtm€ae, B. Paavel, and T. Kauer. (2013). Removing glint effects from field radiometry data measured in optically complex coastal and inland waters. Remote Sens. Environ. 133: 85–89. doi:10.1016/j.rse.2013.02.011

Landis, J. R., Koch, G. G. (1977). An application of hierarchical kappa-type statistics in the assessment of majority agreement among multiple observers. Biometrics, 363-374.

Le, C., Zha, Y., Li, Y., Sun, D., Lu, H., Yin, B. (2010). Eutrophication of lake waters in China: cost, causes, and control. Environmental Management, 45(4), 662-668.

Lee, Z., Carder, K. L., Mobley, C. D., Steward, R. G., Patch, J. S. (1998). Hyperspectral remote sensing for shallow waters. I. A semianalytical model. Applied optics, 37(27), 6329-6338.

Lehner, B., Döll, P. (2004). Global Lakes and Wetlands Database GLWD. GLWD Docu mentation.

Li J., Wu D., Wu Y., Liu H., Shen Q., Zhang H. (2009). Identification of algae-bloom and aquatic macrophytes in Lake Taihu from in-situ measured spectra data. Journal of Lake Sciences, 21(2), 215-222.

Li, J., Wang, S., Wu, Y., Zhang, B., Chen, X., Zhang, F., Shen, Q., Peng, D., Tian, L. (2016). MODIS observations of water color of the largest ten lakes in China between 2000 and 2012. International Journal of Digital Earth, 1-18.

Lillesand, T. M., Johnson, W. L., Deuell, R. L., Lindstrom, O. M., Meisner, D. E. (1983). Use of Landsat data to predict the trophic state of Minnesota lakes.

Lim, A., Hedley, J. D., LeDrew, E., Mumby, P. J., Roelfsema, C. (2009). The effects of ecologically determined spatial complexity on the classification accuracy of simulated coral reef images. Remote Sensing of Environment, 113(5), 965-978.

Liu, C., Frazier, P., Kumar, L. (2007). Comparative assessment of the measures of thematic classification accuracy. Remote sensing of environment, 107(4), 606-616.

Lyzenga, D. R. (1978). Passive remote sensing techniques for mapping water depth and bottom features. Applied optics, 17(3), 379-383.

Ma, S., Tao, Z., Yang, X., Yu, Y., Zhou, X., Li, Z. (2014). Bathymetry retrieval from hyperspectral remote sensing data in optical-shallow water. IEEE Transactions on Geoscience and Remote Sensing, 52(2), 1205-1212.

Matthews, M. W., Odermatt, D. (2015). Improved algorithm for routine monitoring of cyanobacteria and eutrophication in inland and near-coastal waters. Remote Sensing of Environment, 156, 374-382.

McClain, C. R. (2009). A decade of satellite ocean color observations*. Annual Review of Marine Science, 1, 19-42.

Ministry of Environmental Protection of the People's Republic of China (MEPPRC). 2013. China Environmental State Bulletin 2012. http://jcs.mep.gov.cn/hjzl/zkgb/2012zkgb/.

Mobley, C. D., Sundman, L. K. (2003). Effects of optically shallow bottoms on upwelling radiances: Inhomogeneous and sloping bottoms. Limnology and Oceanography, 48(1part2), 329-336.

Mukherjee, M., Ray, A., Post, A. F., McKay, R. M., Bullerjahn, G. S. (2016). Identification, enumeration and diversity of nitrifying planktonic archaea and bacteria in trophic end members of the Laurentian Great Lakes. Journal of Great Lakes Research, 42(1), 39-49.

Okullo, W., Hamre, B., Frette, Ø, Stamnes, J. J., Sørensen, K., Ssenyonga, T. (2011). Validation of MERIS water quality products in Murchison bay, Lake Victoria–preliminary results. International journal of remote sensing, 32(19), 5541-5563.

Olmanson, L. G., Bauer, M. E., Brezonik, P. L. (2008). A 20-year Landsat water clarity census of Minnesota's 10,000 lakes. Remote Sensing of Environment, 112(11), 4086-4097.

O'Reilly, C. M., Alin, S. R., Plisnier, P. D., Cohen, A. S., McKee, B. A. (2003). Climate change decreases aquatic ecosystem productivity of Lake Tanganyika, Africa. Nature, 424(6950), 766-768.

O'Reilly, J.E., Maritorena, S., Mitchell, B. G., Siegel, D. A., Carder, K. L., Garver, S. A., Kahru, M., McClain, C. R. (1998). Ocean color chlorophyll algorithms for SeaWiFS, Journal of Geophysical Research 103, 24937-24953, doi: 10.1029/98JC02160.

Palmer, S. C. J., Kutser, T., Hunter, P. D. (2015). Remote sensing of inland waters: Challenges, progress and future directions. Remote Sensing of Environment, 157, 1-8. doi:10.1016/j.rse.2014.09.021

Papoutsa, C., Akylas, E., Hadjimitsis, D. (2014). Trophic State Index derivation through the remote sensing of Case-2 water bodies in the Mediterranean Region. Open Geosciences, 6(1), 67-78.

Pulliainen, J., Kallio, K., Eloheimo, K., Koponen, S., Servomaa, H., et al. (2001). A semi-operative approach to lake water quality retrieval from remote sensing data. Science of the Total Environment, 268(1), 79-93.

Raji, A. (1993). The past history and present trends in the fisheries of Lake Chad. 213-225.

Rakwatin, P., Takeuchi, W., Yasuoka, Y. (2009). Restoration of Aqua MODIS band 6 using histogram matching and local least squares fitting. IEEE Transactions on Geoscience and Remote Sensing, 47(2), 613-627.

Rimet, F., Bouchez, A., Montuelle, B. (2015). Benthic diatoms and phytoplankton to assess nutrients in a large lake: Complementarity of their use in Lake Geneva (France–Switzerland). Ecological Indicators, 53, 231-239.

Rodhe, W. (1969). Crystallization of eutrophication concepts in northern Europe.

Sass, G. Z., Creed, I. F., Bayley, S. E., Devito, K. J. (2007). Understanding variation in trophic status of lakes on the Boreal Plain: a 20 year retrospective using Landsat TM imagery. Remote Sensing of Environment, 109(2), 127-141.

Shanmugam, P., Ahn, Y. (2007). New Atmospheric Correction Technique to Retrieve the Ocean Colour from Seawifs Imagery in Complexcoastal Waters. Journal of Optics A: Pure and Applied Optics 9: 511–530. doi:10.1088/1464-4258/9/5/016.

Sheela, A. M., Letha, J., Joseph, S. (2011b). Environmental status of a tropical lake system. Environmental monitoring and assessment, 180(1-4), 427-449.

Sheela, A. M., Letha, J., Joseph, S., Ramachandran, K. K., Sanalkumar, S. P. (2011a). Trophic state index of a lake system using IRS (P6-LISS III) satellite imagery. Environmental monitoring and assessment, 177(1-4), 575-592.

Shen, Q., Li, J. S., Wu, Y. H., Zhang, B. (2014). Review of spectral curve fitting and analysis of inherent optical parameters in lakes. Remote Sensing Information, 29

(4): 112-125.

Sheng, H.， Wu, Z., Liu, M., et al. (2015). Water quality trends in recent 10 years and correlation with hydro-meteorological factors in Xin'anjiang Reservoir． Acta Scientiae Circumstantiae, 35(1): 118-127.

Shi, K., Zhang, Y., Zhu, G., Liu, X., Zhou, Y., Xu, H., et al. (2015). Long-term remote monitoring of total suspended matter concentration in Lake Taihu using 250m MODIS-Aqua data. Remote Sensing of Environment, 164, 43-56.

Shi, W., Wang M. (2009). An assessment of the black ocean pixel assumption for MODIS SWIR bands. Remote sensing of environment 113(8): 1587-1597.

Shuchman, R. A., Leshkevich, G., Sayers, M. J., Johengen, T. H., Brooks, C. N., Pozdnyakov, D. (2013). An algorithm to retrieve chlorophyll, dissolved organic carbon, and suspended minerals from Great Lakes satellite data. Journal of Great Lakes Research, 39, 14-33.

Singh, S.P. and Singh, P. (2015). Effect of temperature and light on the growth of algae species: a review. Renewable and Sustainable Energy Reviews, 50, pp.431-444.

Smith, V. H. (2003). Eutrophication of freshwater and coastal marine ecosystems a global problem. Environmental Science and Pollution Research, 10(2): 126-139.

Song, K., Ma, J., Wen, Z., Fang, C., Shang, Y., Zhao, Y., Du, J. (2017). Remote estimation of K d (PAR) using MODIS and Landsat imagery for turbid inland waters in Northeast China. ISPRS Journal of Photogrammetry and Remote Sensing, 123, 159-172.

Spyrakos, E., O'Donnell, R., Hunter, P.D., Miller, C., Scott, M., Simis, S.G., Neil, C., Barbosa, C.C., Binding, C.E., Bradt, S. and Bresciani, M. (2018). Optical types of inland and coastal waters. Limnology and Oceanography, 63(2), pp.846-870.

Stich, H. B., Brinker, A. (2010). Oligotrophication outweighs effects of global warming in a large, deep, stratified lake ecosystem. Global Change Biology, 16(2), 877-888.

Strahler, A., Muchoney, D., Borak, J., Friedl, M., Gopal, S., Lambin, E., Moody, A., (1999). MODIS Land Cover Product: Algorithm Theoretical Basis Document (ATBD), Version 5.0. Boston University, Boston, MA, 72 p.

Stuart H. Hurlbert. (1991).Saline Lakes V, Proceedings of the Vth International Symposium on Inland Saline Lakes, held in Bolivia, 22–29 March 1991.

Tang, J. W., Tian, G. L., Wang, X. Y., Wang, X. M., Song, Q. J. (2004). The methods of water spectra measurement and analysis I: above-water method. Journal of Remote Sensing, 8(1), 37-44.

Thiemann, S., Kaufmann, H. (2000). Determination of chlorophyll content and trophic state of lakes using field spectrometer and IRS-1C satellite data in the Mecklenburg Lake District, Germany. Remote Sensing of Environment, 73(2), 227-235.

USEPA. (2009). National Lakes Assessment: A collaborative survey of the Nation’s Lakes. EPA 841-R-09-001. U.S. Environmental Protection Agency, Office of Water and Office of Research and Development, Washington, D.C. https://nationallakesassessment.epa.gov/

USEPA. (2016). National Lakes Assessment 2012: A collaborative survey of lakes in the United States. EPA 841-R-16-113. U.S. Environmental Protection Agency, Washington, DC. https://nationallakesassessment.epa.gov/

Vant, W. N. (Ed.). (1987). Lake managers handbook: a guide to undertaking and understanding investigations into lake ecosystems, so as to assess management options for lakes (No. 103). Published for the National Water and Soil Conservation Authority by the Water and Soil Directorate, Ministry of Works and Development.

Velpuri, N. M., Senay, G. B., Asante, K. O. (2012). A multi-source satellite data approach for modelling Lake Turkana water level: calibration and validation using satellite altimetry data. Hydrology and Earth System Sciences, 16(1), 1-18.

Verburg, P. (2006). The need to correct for the Suess effect in the application of δ13C in sediment of autotrophic Lake Tanganyika, as a productivity proxy in the Anthropocene. Journal of Paleolimnology, 37(4): 591-602.

Verburg, P., Hamill, K., Unwin, M., Abell, J. (2010). Lake water quality in New Zealand 2010: Status and trends. NIWA client report HAM, 107.

Vermote, E., Vermeulen A. (1999). Atmospheric correction algorithm: spectral reflectances (MOD09), ATBD version 4. https://eospso.gsfc.nasa.gov/sites/default/files/atbd/atbd_mod08.pdf. (Accessed April 1999).

Vermote, E. F., Roger, J. C., Ray, J. P. (2015). MODIS Surface Reflectance User's Guide-Collection 6. In Tech. Rep. Version 1.4, NASA GSFC Terrestrial Information Systems Laboratory, MODIS Land Surface Reflectance Science Computing Facility. Greenbelt, USA.

Vollenweider, R. A. (1981). Eutrophication- a Global Problem. Water Qual. Bull., 6(3), 59-62.

Vollenweider, R. A., Kerekes, J. (1982). Eutrophication of waters. Monitoring, assessment and control. Organization for Economic Co-Operation and Development (OECD), Paris, 156.

Wang, L., Qu, J. J., Xiong, X., Hao, X., Xie, Y., Che, N. (2006). A new method for retrieving band 6 of Aqua MODIS. IEEE Geoscience and Remote Sensing Letters, 3(2), 267-270.

Wang, M., and W. Shi. (2007).The NIR-SWIR Combined Atmospheric Correction Approach for MODIS Ocean Color Data Processing. Optics Express 15: 15722–15733. doi:10.1364/OE.15.015722.

Wang, M., Shi, W., Tang, J. (2011). Water property monitoring and assessment for China's inland Lake Taihu from MODIS-Aqua measurements. Remote Sensing of Environment, 115(3), 841-854.

Wang, S. M., Dou, H. S. (1998). Chinese Lakes. Science Press, Beijing.

Wang, S., Li, J., Shen, Q., Zhang, B., Zhang, F., Lu, Z. (2015). MODIS-based radiometric color extraction and classification of inland water with the Forel-Ule Scale: A Case Study of Lake Taihu. IEEE Journal of Selected Topics in Applied Earth Observations and Remote Sensing, 8(2), 907-918.

Wang. S., Li, J., Zhang, B., Shen, Q., Zhang, F., Lu, Z. (2016). A simple correction method for the MODIS surface reflectance product over typical inland waters in China, International Journal of Remote Sensing, 37:24, 6076-6096.

Wang, Z., Hong, J., Du, G. (2008). Use of satellite imagery to assess the trophic state of Miyun Reservoir, Beijing, China. Environmental Pollution, 155(1), 13-19.

Wernand, M. R., Van der Woerd, H. J. (2010). Spectral analysis of the Forel-Ule Ocean colour comparator scale. Journal of the European Optical Society-Rapid Publications, 5.

Wernand, M. R., Hommersom, A., Van der Woerd, H. J. (2013a). MERIS-based ocean colour classification with the discrete Forel-Ule scale. Ocean Science 9: 477-487.

Wernand, M.R., Van der Woerd, H.J., Gieskes, W.W.C. (2013b). Trends in Ocean Colour and Chlorophyll Concentration from 1889 to 2000, Worldwide. PLoS ONE 8(6): e63766. doi:10.1371/journal.pone.0063766

Williams, W. (2002). Environmental threats to salt lakes and the likely status of inland saline ecosystems in 2025. Environmental Conservation, 29(2), 154-167. doi:10.1017/S0376892902000103

Van der Woerd, H. J., Wernand, M. R. (2015). True colour classification of natural waters with medium-spectral resolution satellites: SeaWiFS, MODIS, MERIS and OLCI. Sensors, 15(10), 25663-25680.

Van der Woerd H.J. et al., (2016).True color analysis of natural waters with SeaWiFS, MODIS, MERIS and OLCI by SNAP. Presented at Ocean Optics conference, At Victoria BC Canada, Volume: XXIII.

Wu, G., Cui, L., He, J., Duan, H., Fei, T., Liu, Y. (2013). Comparison of MODIS-based models for retrieving suspended particulate matter concentrations in Poyang Lake, China. International Journal of Applied Earth Observation and Geoinformation, 24, 63-72.

Wu, G., De Leeuw, J., Skidmore, A. K., Prins, H. H., Liu, Y. (2008). Comparison of MODIS and Landsat TM5 images for mapping tempo–spatial dynamics of Secchi disk depths in Poyang Lake National Nature Reserve, China. International Journal of Remote Sensing, 29(8), 2183-2198.

Xiang, B., Song, J. W., Wang, X. Y., Zhen, J. (2015). Improving the accuracy of estimation of eutrophication state index using a remote sensing data-driven method: A case study of Chaohu Lake, China. Water SA, 41(5), 753-761.

Yang, L., Lei, K., Meng, W., Fu, G., Yan, W. (2013). Temporal and spatial changes in nutrients and chlorophyll-α in a shallow lake, Lake Chaohu, China: An 11-year investigation. Journal of Environmental Sciences, 25(6), 1117-1123.

Ylöstalo, P., Kallio, K., Seppälä, J. (2014). Absorption properties of in-water constituents and their variation among various lake types in the boreal region. Remote Sensing of Environment, 148, 190-205.

Zhang, F., Li, J., Zhang, B., Shen, Q., Ye, H., Wang, S., Lu, Z. (2018). A simple automated dynamic threshold extraction method for the classification of large water bodies from landsat-8 OLI water index images. International Journal of Remote Sensing, 39(11), 3429-3451.

Zhang, M., R. Ma, J. Li, B. Zhang, and H. Duan. (2014). A Validation Study of an Improved SWIR Iterative Atmospheric Correction Algorithm for MODIS-Aqua Measurements in Lake Taihu, China. IEEE Transactions on Geoscience and Remote Sensing 52 (8): 4686–4695. doi:10.1109/TGRS.2013.2283523.